View Article Online
View Journal

Nanoscale Horizons

The home for rapid reports of exceptional significance in nanoscience and nanotechnology

Accepted Manuscript

This article can be cited before page numbers have been issued, to do this please use: G. Lin, J. Huang, X. Li, Y. LIU, T. Juenke, A. Finstad and M. Zhang, *Nanoscale Horiz.*, 2025, DOI: 10.1039/D5NH00299K.

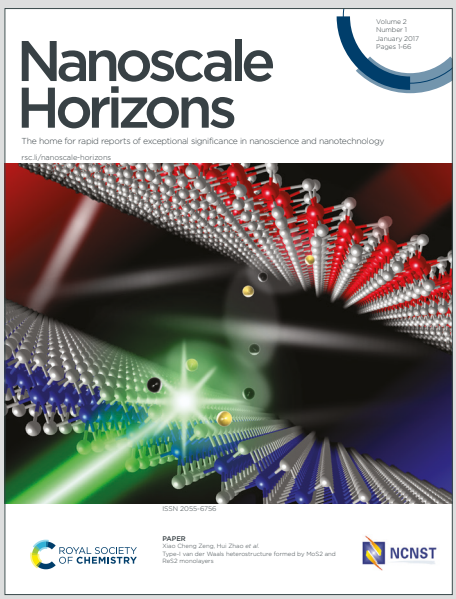

View Article Online
DOI: 10.1039/D5NH00299K

ARTICLE

A Modular Polymer Platform for Efficient mRNA Delivery in Cancer Immunotherapy

Guanyou Lin†[a], Jianxi Huang†[a], Xinqi Li[a], Yunshan Liu[a], Taylor Juenke[a], Arthur Finstad[a] and Miqin Zhang[a*]

Received 00th January 20xx,
Accepted 00th January 20xx

DOI: 10.1039/x0xx00000x

The use of mRNA for prophylactic and therapeutic applications, such as treating the coronavirus pandemic and cancer, has garnered significant attention. However, mRNA's inherent liability requires robust delivery platforms to enable effective mRNA-based therapies. While lipid nanoparticles (LNPs) have shown success in mRNA delivery, they face challenges in safety, storage and manufacturing costs. Polymeric mRNA delivery platforms have emerged as promising alternatives due to their structural versatility, durability, and transfection efficiency. This study presents PFHA-PEI-mRNA-HP, a polymeric mRNA delivery nanoplatform that utilizes simultaneous fluorination and heparinization of low molecular weight polyethylenimine (PEI)-based mRNA complexes to enhance performance. These modifications, applied to the PEI backbone, significantly improved the physicochemical properties, cellular uptake, endosomal escape capability, and biocompatibility of the platform, resulting in a substantial increase in transfection efficiency. PFHA-PEI-mRNA-HP achieved ultra-high transfection efficiency of >90% across multiple cancer cell types, outperforming the LNP-based delivery reagent, Lipofectamine 2000. Additionally, PFHA-PEI-mRNA-HP demonstrated superior stability compared to Lipofectamine 2000 when stored above 0 °C for 15 days. When loaded with therapeutic IL12 mRNA, PFHA-PEI-mRNA-HP effectively delivered its payload in vivo and, in combination with anti-PD-L1 therapy, significantly inhibited tumor growth in a triple-negative breast cancer mouse model without causing harm to healthy tissues. These results highlight PFHA-PEI-mRNA-HP as a highly efficient and reliable mRNA delivery platform for cancer gene therapies.

New Concepts

This research presents an innovative polymeric mRNA delivery platform that addresses key limitations of lipid nanoparticles (LNPs), widely used in mRNA therapeutics. Despite their clinical success, LNPs rely on complex multicomponent lipid formulations, labor-intensive screening, and cold-chain storage, resulting in batch inconsistencies and high costs. Limited lipid reactive sites also restrict functionalization for targeted therapies. PFHA-PEI-mRNA-HP, based on a single, fluorinated, and heparinized low molecular weight PEI macromolecule, forms cationic nanoparticles that self-assemble with mRNA via simple mixing, enhancing scalability, affordability, and consistency. Fluorination boosts cellular uptake and endosomal escape, while heparinization improves biocompatibility and stability. The platform outperforms Lipofectamine 2000 in transfection efficiency across cancer cell lines and remains stable without cold storage. In vivo, it effectively delivers IL12 mRNA, suppressing triple-negative breast cancer in mice alongside anti-PD-L1 therapy without toxicity. This study not only provides insights of designing and optimizing a novel polymeric mRNA delivery platform but also conceptually demonstrated the promising utility of functionalized cationic polymers in the field of mRNA delivery.

1. Introduction

Messenger RNA (mRNA), the intermediator between the fixed genetic blueprint (DNA) and the terminal effector (proteins), offers great flexibility and utility as a medicinal agent.[1] The delivery of prophylactic mRNA payloads via nanomaterial-based platforms has shown its technological prowess in addressing the significant public health challenges the world is facing during recent pandemic years. Successful mRNA transfection can express virtually any proteins of design in cells and tissues to manipulate cell behaviors and exert prophylactic or therapeutic effects to treat or prevent diseases. The cytosolic mRNA activity which eliminates the need to pass cell's nuclear envelope barrier for transient protein expression and the risk of insertional mutagenesis enables facile and safe transfection.[2] Due to mRNA's labile nature, however, the main challenge of mRNA delivery lies with a reliable carrier offering protection from enzymatic and chemical degradation while ferrying mRNA across biological barriers. While lipid nanoparticles (LNPs) have achieved remarkable success as a mRNA delivery platform for vaccines and treatments, there is still room for improvement to address the safety concerns associated with LNP-mRNA formulations. These formulations may pose limitations and potential side effects when applied clinically.[3-5] Recent findings also pointed out that LNP not only encapsulates mRNA but also water pockets which could readily subject mRNA to hydrolysis and jeopardize mRNA's structural integrity unless stored at ultra-cold conditions (–20 °C to –80 °C).[6-8] The manufacture of LNP-mRNA requires meticulous mixing of many different lipid

[a]Department of Materials Science and Engineering, University of Washington, Seattle, Washington 98195, United States. E-mail: mzhang@uw.edu
†These authors contributed equally.
Electronic Supplementary Information (ESI) available: [details of any supplementary information available should be included here]. See DOI: 10.1039/x0xx00000x

constituents (usually four) with mRNA in aqueous-organic solvent mixtures, commonly using water-ethanol, in high precision mixing platforms, such as rapid microfluidic mixing devices, to ensure reproducibility.[9, 10] To equip LNP with active tumor targeting, additional reactive lipids would need to be added to LNP for post-synthetic ligand installation, which could further complicate LNP's manufacture process and alter LNPs' structural integrity which is largely based on weak electrostatic and hydrophobic interactions.[11] Therefore, there is a fervor need for a novel class of mRNA delivery platforms which can build upon LNP's success while addressing its limitations. Efforts of modifying LNP with polymeric moieties to improve its mRNA delivery performance have been reported in recent years.[12, 13]

Cationic polymer-based mRNA delivery platforms have also gained extensive recognition in research. Different from LNP, a cationic polymer can be simultaneously equipped with multiple functional moieties so that only very few polymeric constituents are needed to form nanoparticle (NP) with mRNA, making the production of polymeric mRNA NPs much easier and less costly than that of LNP-mRNA.[10] Due to their larger-than-lipid molecular weight and abundance in positive charge, cationic polymers can form more robust and stable complex with mRNA which can better protect mRNA from degradation than lipids via multivalent electrostatic condensation.[14] Among innumerous types of cationic polymers, only polyethyleneimine (PEI) is widely applied to deliver mRNA due to its superior capability of mRNA condensation and endosomal escape.[15] To circumvent large molecular weight PEI's non-biodegradability and cytotoxicity issues, low molecular weight branched PEI-based delivery platforms have been developed and showed great efficacies in delivering mRNA for vaccination against HIV and influenza viruses as well as treating muscle dystrophy, demonstrating low molecular weight branched PEI's utility and suitability for mRNA delivery applications.[16-19] However, the mRNA transfection efficiency of these mRNA delivery platforms was either inferior to that of LNP or only compared to that of the toxic high molecular weight PEI, leaving low molecular weight PEI-based mRNA delivery platform's transfection efficiency still in doubt.

Fluorine has been widely utilized in medicinal industry to modify drugs' molecular structures for better pharmacokinetic and therapeutic outcomes and imaging application purposes.[20-23] In the context of biomaterials, fluorination—typically achieved by incorporating fluorocarbon moieties into polymer structures—has recently been shown to substantially improve the gene delivery efficiency of cationic polymers.[24-27] This enhancement rises from several key properties of fluorocarbons. First, fluorinated chains exhibit amphiphobicity—they are both hydrophobic and lipophobic—leading to low interfacial energy and reduced nonspecific interactions with proteins and membranes.[28, 29] Second, fluorocarbon-modified polymers have a strong tendency to self-assemble into compact and stable nanostructures, which improves mRNA condensation and protects against enzymatic degradation.[30] Third, fluorinated polymers facilitate crossing biological barriers, such as the plasma membrane and endosomal compartments, by promoting membrane destabilization and escape.[31-33] These combined effects, including enhanced stability, reduced nonspecific adsorption, and improved intracellular trafficking, make fluorinated cationic polyplexes promising carriers for nucleic acid delivery. Fluorinated cationic polyplexes have been reported to have high efficiency in delivering DNA,[24, 25], siRNA[34, 35] and proteins[36], but it has been rarely reported for mRNA delivery.

A common dilemma for polymeric gene delivery platforms is that the high density of cationic charges necessary for effective nucleic acid condensation also poses issues of toxicity, insufficient nucleic acid release and serum protein adsorption. A promising solution for these problems is embellishing cationic polyplexes with polyanions. Adding polyanions not only improves complex's biocompatibility and serum stability by partially shielding complex's positive surface charge but also helps tune the binding tightness between cationic polymers and nucleic acids so that a subtle packing-unpacking balance can be achieved for efficient nucleic acid release.[37, 38] As a biocompatible polysaccharide with high anionic charge density, heparin (HP) has been repeatedly reported to significantly improve various types of cationic polyplexes' biocompatibility, nucleic acid release profile and transfection efficiency when incorporated.[39-41] Although the polyanion embellishment strategy has been proven effective for DNA and RNAi delivery, whether the same strategy would display similar enhancement effect on mRNA delivery platforms remained largely unexplored, if not completely unknown.

By combining the merits of low molecular weight branched PEI, fluorination, and heparin embellishment, polymeric mRNA NP could yield comparable to or even better mRNA delivery efficiency than LNP while possessing superior structural integrity compatible with post-synthetic modifications such as targeting ligand conjugation, more robust storage stability, and simplified yet reproducible manufacture process. To this end, we introduced a polymeric NP mRNA delivery platform (termed PFHA-PEI-mRNA-HP) and demonstrated its utility in transfection of multiple cancer types. Branched PEI with 2 kDa molecular weight, perfluoroheptanoic acid (PFHA) as the fluorocarbon moiety, and low molecular weight (1.8 kDa–7.5 kDa) heparin (HP) were selected as the constituents of this mRNA delivery platform. PFHA-PEI-mRNA-HP possessed a sub-hundred nm size, spherical shape and sufficient positive surface charge which are conducive for effective mRNA delivery. Since the capability of achieving successful gene delivery in cancer cells is crucial in improving the therapeutic outcomes of cancer treatments, PFHA-PEI-mRNA-HP was applied to different types of cancer cells to test its in vitro mRNA delivery utility. Breast and liver cancer cells were chosen as the target cells as they are major types of cancers inflicting large number of deaths worldwide (over 1.5 millions in 2020).[42] Brain cancer cells were also tested because brain cancer is one the deadliest cancer types with a 5-year survival rate below 5% even though it is not as prevalent as breast and liver cancers.[43]

Notably, PFHA-PEI-mRNA-HP was able to achieve ultra-high mRNA transfection efficiency (>90%) across breast cancer cells, brain cancer cells and liver cancer cells while showing innocuous toxicity profiles on these cell lines. PFHA-PEI-mRNA-HP exhibited a stability superior to Lipofectamine 2000-mRNA LNP when stored at 4°C for 15 days. Loaded with immunotherapeutic interleukin 12 (IL12) mRNA, PFHA-PEI-mRNA-HP has demonstrated promising utilities in inducing antitumor immunity to suppress the growth of metastatic triple negative breast cancer (TNBC) tumors *in vivo*, without causing harm to healthy tissues. The mRNA delivery performance and storage stability demonstrated that PFHA-PEI-mRNA-HP can be a highly efficient and reliable mRNA delivery platform for gene therapy against aggressive solid tumors and other diseases.

2. Materials and Methods

2.1 Materials

CleanCap® EGFP mRNA was purchased from TriLink Biotechnologies (San Diego, CA, USA). Low molecular weight heparin was purchased from Galen Laboratory Supplies (North Haven, CT, USA). Branched PEI (MW 2 kDa) was purchased from Polysciences (Warrington, PA, USA). Microliter syringes (100 µL max volume) and removable needles (32 gauge, point style 3) were purchased from Hamilton (Reno, NV, USA). NE-300 "Just Infusion"™ Syringe Pump was purchased from New Era Pump System Inc. (Farmingdale, NY, USA). (1-Ethyl-3-[3-dimethylaminopropyl] carbodiimide hydrochloride (EDC), N-hydroxysuccinimide (NHS), Lab-Tek™ II 8-well chambered coverglass, NucBlue DAPI reagent, Lipofectamine 2000, LysoTracker™ Red DND-99, ultrapure agarose, antibiotic-antimycotic (100X), Tryple Express Enzyme solution, RPMI 1640 and DMEM cell culture medium were purchased from Invitrogen (Carlsbad, CA, USA). HyClone characterized fetal bovine serum (FBS) were purchased from GE Healthcare Life Sciences (Pittsburgh, PA, USA). Label IT Tracker Intracellular Nucleic Acid Labeling Kits were purchased from Mirus Bio (Madison, WI, USA). Single Strand RNA ladder was purchased from New England Biolabs (Ipswich, MA, USA). SpectraPOR7 dialysis membrane was purchased from Repligen Corp (Waltham, MA, USA). Calcein AM Viability dye and propidium iodide were purchased from Thermofisher Scientific (Waltham, MA, USA). All other chemicals were purchased from Sigma-Aldrich (St Louis, MO, USA). 4T1, HepG2, MCF7, SF763 and C6 cell lines were purchased from American Type Culture Collection (Manassas, VA, USA). M6 cell line was kindly shared by the Disis group from Cancer Vaccine Institute at UW Medicine. IL12 DNA (Tandem p40p35) was a gift from Nevil Singh (Addgene plasmid # 108665).

2.2 Synthesis of PFHA-PEI

PFHA was conjugated onto PEI via EDC/NHS coupling chemistry. 127.4 mg of PFHA, 80.5 mg of EDC and 58.1 mg of NHS were separately dissolved in methanol at 50 mg/mL concentration. PFHA, EDC and NHS solutions were mixed together by adding EDC and subsequently NHS to PFHA solution. The mixed solution was placed on a rocker and incubated for 3 hours at room temperature. Next, 100 mg branched PEI was dissolved in methanol at 50 mg/mL and added to the PFHA-EDC-NHS mixture solution and rocked at room temperature for 16 hours. The resultant solution was dialyzed against Milli-Q water for 2 days using 1k MWCO SpectraPOR7 dialysis membrane. The dialyzed solution was centrifuged at 4000G for 5 mins to precipitate out large aggregates. The clear supernatant was then freeze-dried and stored at –20 °C for long term storage. The typical yield of a PFHA-PEI batch is around 60% of the combined mass of all the reactants.

2.3 FTIR Spectra Collection

2 mg of each of the PFHA, PEI and PFHA-PEI dry samples were mixed with 200 mg of KBr and pulverized into fine powders, and a pellet was prepared for characterization. FTIR spectra were obtained using a Nicolet 5-DXB FTIR spectrometer (ThermoFisher, Boston, MA) with a resolution of 4 cm^{-1} and averaging 64 runs.

2.4 XPS Spectra Analysis

X-ray photoelectron spectroscopy (XPS, AXIS Ultra DLD / Surface Science Instruments S-Probe, Kratos) was performed to study the amide group (O=C-NH-) formation. This instrument has a monochromatized Al Kα X-ray and a low-energy electron flood gun for charge neutralization. The X-ray spot size for these acquisitions was on the order of 700 x 300 µm. The electrostatic lens was used for data collection. The pressure in the analytical chamber during spectral acquisition was less than 5 x 10^{-9} Torr. The pass energy for survey spectra (composition) was 160 eV. The pass energy for the high-resolution spectra was 40 eV. The take-off angle (the angle between the sample normal and the input axis of the energy analyzer) was 0° (0-degree take-off angle ~ 100 Å sampling depth). The Kratos Vision2 software was used to determine the peak areas and to calculate the elemental compositions from the peak areas. CasaXPS was used to peak fit the high-resolution spectra. For the high-resolution spectra, a Shirley background was used, and all binding energies were referenced to the C ls C-C bonds at 285.0 eV.

2.5 Formation of PFHA-PEI-mRNA-HP Complex

PFHA-PEI was redissolved in Milli-Q water at 10 mg/mL and was centrifuged at 16,000 G for 10 mins to eliminate possible large aggregates. The supernatant from PFHA-PEI was diluted to 7.5 mg/mL by 20 mM Hepes buffer (pH 7.4). mRNA was diluted to 0.5 mg/mL in 20 mM Hepes buffer (pH 7.4). HP was dissolved in 20 mM Hepes buffer (pH 7.4) at 0.5 mg/mL concentration. To make a PFHA-PEI-mRNA complex, 5 µL of mRNA solution was mixed with 5 µL of PFHA-PEI solution via the RSM device. Specifically, 5 µL of PFHA-PEI solution was first added to the bottom of a 0.6 mL microtube and 5 µL of mRNA solution was loaded into a Hamilton microliter syringe. mRNA solution was then slowly injected into PFHA-PEI solution at the flow rate of 1 µL/s controlled by a syringe pump while the PFHA-PEI solution was being stirred by a rotor tip at 500 RPM to ensure homogenous mixing. To add HP to PFHA-PEI-mRNA complex, desired amount of HP was loaded into a Hamilton microliter syringe and slowly injected into PFHA-PEI-mRNA solution at the flow rate of 0.5 µL/s controlled by a syringe pump while the PFHA-PEI-mRNA solution was being stirred by a rotor tip at 500 RPM to ensure homogenous mixing. For making the PEI-mRNA complex, PEI was first dissolved in 20 mM Hepes buffer (pH 7.4) at 7.5 mg/mL concentration followed by the same mixing procedure as that of making PFHA-PEI-mRNA complex.

2.6 Hydrodynamic Size, Serum Stability and Zeta Potential Measurement

The hydrodynamic size and zeta potential of PEI-mRNA, PFHA-PEI-mRNA and PFHA-PEI-mRNA-HP (with varying HP amounts) were determined using a Zetasizer Nano-ZS (Malvern Instruments, Worcestershire, UK). The measurements were performed in 20 mM HEPES buffer (pH 7.4) at room temperature. To test samples' serum

stability, the samples were diluted 100 times with PBS supplemented with 10% fetal bovine serum (FBS) and placed in a 37°C water bath. Hydrodynamic size measurements were made at various time points within 3 weeks.

2.7 Gel Electrophoresis Retardation Assay

Free mRNA, PEI-mRNA, PFHA-PEI-mRNA and PFHA-PEI-mRNA-HP (with varying HP amounts) samples were added to 1% agarose gel at 1 μg mRNA per lane. Gel electrophoresis was run for about 30 min at 120 V. Gels were stained with 0.5 μg/mL ethidium bromide and visualized using a Bio-Rad Universal Hood II Gel Doc System.

2.8 TEM Imaging

TEM samples were prepared by the addition of 4 μL of PEI-mRNA, PFHA-PEI-mRNA or PFHA-PEI-mRNA-HP (with varying HP amounts) solution to a Formvar/carbon coated 300-mesh copper grid (Ted Pella, Inc., Redding, CA) and stained with 1% uranyl acetate and subsequently allowed to air dry. TEM images were acquired on a Tecnai G2 F20 electron microscope (FEI, Hillsboro, OR) operating at a voltage of 200 kV.

2.9 Cell Culture

4T1 and M6 mouse breast cancer cells were cultured in RPMI1640 medium supplemented with 10% vol/vol FBS and 1% vol/vol antibiotic–antimycotic. MCF7 human breast cancer cells, HepG2 human liver cancer cells, SF763 human glioblastoma cells and C6 rat glioma cells were cultured in DMEM medium supplemented with 10% vol/vol FBS and 1% vol/vol antibiotic–antimycotic. Culture media were replenished once every three days if cells are not confluent enough to be passaged. When cell density reached 80%, 4T1, MCF7, HepG2, SF763 and C6 cells were dissociated with TrypLE agent, M6 with PBS + 2.5% v/v EDTA. Dissociated cells were suspended in their corresponding culture media and pelleted at 500 G for 5 mins. The desired number of cells were then transferred to new culture flasks with fresh culture media. Cultures were maintained in a 37 °C and 5% CO2 humidified incubator.

2.10 Cellular Uptake and Endosomal Escape Studies

mRNA was labeled with Cy5 following the manufacturer's protocol of the Label IT Tracker Intracellular Nucleic Acid Labeling Kit before complexed into PEI-mRNA, PFHA-PEI-mRNA and PFHA-PEI-mRNA-HP. 4T1, M6 and HepG2 cells were seeded at 15,000 cells per well in 8-well glass chambers. All cells were incubated for 24 hours before treatments were added. PEI-mRNA, PFHA-PEI-mRNA and PFHA-PEI-mRNA-HP were then added to cells at 2 μg/mL mRNA concentration, incubated for either 2 hours or 12 hours before adding 75 nM of Lysotracker Red DND reagent, and then incubated for another 1 hour. There were two identical sets of samples for the 12-hour time point experiment, among which one set was incubated normally in 37 °C incubator while another set was incubated in refrigerator at 4 °C. The refrigerated sample was briefly placed at room temperature for adding Lysotracker reagent and was immediately returned to 4 °C for 1 hour incubation. All cells were then washed three times with cold PBS and fixed with paraformaldehyde (4% in PBS) for 15 mins at room temperature. The fixed cells were further washed with cold PBS three times. NucBlue FixCell ReadyProbe DAPI reagent was diluted 10 times in cold PBS and 100 μL was added to each well. Confocal images were acquired using a Leica SP8X confocal laser scanning microscope (Leica, Germany).

2.11 In Vitro Cell Transfection

4T1, M6 and C6 cells were seeded at 4,000 cells per well in 96-well plates. MCF7, HepG2 and SF763 were seeded at 8,000 cells per well in 96-well plates. All cells were incubated for 24 h after seeded on plates before treatments were added. PEI-mRNA, PFHA-PEI-mRNA, PFHA-PEI-mRNA-HP or Lipofectamine 2000-mRNA complexes were added to 100 μL of fully supplemented culture medium to give a final mRNA concentration of 2 μg/mL in each well for all cancer cell lines. The cells were incubated with complexes for 48 h and the cell culture media were replenished after 24 h. For the FGFR inhibition study, cells in the treatment group were pre-incubated with 500 nM PD173074 (FGFR inhibitor, ≥99% purity, purchased from Fisher Scientific, Cat# 506911) for 1 hour prior to transfection. The inhibitor remained present in the medium throughout the 48 h transfection period. Transfection using the commercial agent, Lipofectamine 2000, was performed following the manufacturer's protocol. The cells were imaged 48 h post-transfection with a Nikon TE300 inverted fluorescent microscope (Nikon, Tokyo, Japan).

2.12 Quantitative Analysis of Transfection via Flow Cytometry

After cells have been transfected following the in vitro cell transfection procedures, 40 μL TrypLE was added to each well and the wells were incubated for 8 mins to dissociate adherent cells. 100 μL cold PBS was then added to the trypsinized wells to resuspend cells. The cell suspension was collected in 1.5 mL microtubes and centrifuged at 4 °C at 500 G for 5 mins to pellet cells. Cell pellets were then resuspended in 200 μL cold PBS and transferred to flow cytometry tubes for immediate flow cytometry analysis on FACSCanto II (BD Biosciences) from which data was post-processed using FlowJo software (Treestar, Inc., San Carlos, CA).

2.13 *In vitro* Cell Viability Studies

4T1, M6 and HepG2 cells were seeded at 4,000, 4,000, 8,000 cells per well in 96-well plates, respectively. All cells were incubated for 24 h after seeded on plates before treatments were added. The cells were then treated with PEI-mRNA, PFHA-PEI-mRNA, PFHA-PEI-mRNA-HP or Lipofectamine 2000-mRNA at mRNA concentrations of 0, 0.5, 1, 2, 3 μg/mL. The cells were treated for 24 h before the cell viability was determined using the Alamar Blue assay. The fluorescent signal readout was obtained by a SpectraMax i3 microplate reader (Molecular Devices, Sunnyvale, CA, USA) with 550 nm excitation and 590 nm emission. The fluorescence intensities of all the treatment

groups were normalized so that the viability of the untreated cell group was 100%.

2.14 Functionality Test After Above 0 °C Storage

PFHA-PEI-mRNA-HP and Lipofectamine 2000-mRNA complexes were prepared on day 0 and were kept in storage at 4 °C throughout this study. 4T1 and HepG2 cells were seeded at 4,000 and 12,000 cells per well in 96-well plates respectively. All cells were incubated for 24 h after seeded on plates before treatments were added. PFHA-PEI-mRNA-HP and Lipofectamine 2000-mRNA complexes were added to 100 µL of fully supplemented culture media to give a final mRNA concentration of 2 µg/mL in each well on day 0, 1, 2, 3, 4, 7, 15 after sample preparations. The cells were incubated with complexes for 24 h before imaged with a Nikon TE300 inverted fluorescent microscope (Nikon, Tokyo, Japan).

2.15 In vitro transfection of IL12 mRNA

IL12 mRNA was synthesized from mouse IL12-encoding plasmid DNA obtained from Addgene (Plasmid #108665). The plasmid DNA was transcribed with HiScribe® T7 ARCA mRNA Kit (New England Biolabs Inc, Ipswich, MA) and then purified with Monarch RNA cleanup kit (New England Biolabs Inc, Ipswich, MA). To evaluate the transfection efficiency of PFHA-PEI-mRNA-HP for IL12 mRNA delivery, 4T1 cells were seeded in a 96-well plate at a density of 4 × 10^3 cells per well and incubated at 37°C with 5% CO2 overnight. Cells were then transfected with PFHA-PEI-mRNA-HP complexes loaded with IL12 mRNA, following the same transfection protocol described in Section 2.11. At 2/12/24 hours post-transfection, cells were processed for immunofluorescence staining to visualize IL12 protein expression. For immunostaining, the culture medium was aspirated, and cells were washed with 200 µL of phosphate-buffered saline (PBS) per well. Cells were fixed with 100 µL of 4% paraformaldehyde (PFA) for 10 minutes at room temperature, followed by additional PBS wash. To allow for intracellular staining, cells were incubated with 100 µL of 1X intracellular staining permeabilization wash buffer (Biolegend, Cat. No. 421002) for 10 minutes at room temperature. After washing with PBS, 100 µL of PE-conjugated anti-mouse IL12 antibody (2 µg/mL in PBS) was added to each well, and the plate was incubated at 4°C for 30 minutes. Cells were washed twice, followed by the addition of 100 µL of NucBlue® DAPI reagent (diluted 1:10 in PBS) to stain nuclei. The plate was stored at 4°C, protected from light, until imaging. Fluorescence imaging was performed using a Nikon TE300 inverted fluorescent microscope (Tokyo, Japan). IL12 expression was detected using the PE channel, and cell nuclei were visualized in the DAPI channel.

2.16 In vivo Therapeutic Efficacy and Biosafety Profile Studies of PFHA-PEI-mRNA-HP

All animal studies were conducted in compliance with institutional guidelines and approved by the Institutional Animal Care and Use Committee (IACUC). Female BALB/c mice (6–8 weeks old) were used to establish the 4T1 triple-negative breast cancer (TNBC) model. A total of 4.75×10^5 4T1 cells were resuspended in phosphate-buffered saline (PBS) and subcutaneously inoculated into the right scapular region of each mouse on day 0.

To assess in vivo mRNA delivery, 4T1 tumor-bearing mice (n=3 on day 21) received a single peritumoral subcutaneous injection of PFHA-PEI-mRNA-HP loaded with luciferase mRNA (Luc mRNA) near the tumor site. At 4 hours post-injection, mice were administered luciferin substrate (6 mg for each mouse) via intraperitoneal injection and imaged using an IVIS Spectrum in vivo imaging system to detect bioluminescence.

For therapeutic evaluation, mice were randomly assigned to treatment groups (n=5). On day 3, mice received a 100 µL subcutaneous injection of PFHA-PEI-mRNA-HP loaded with IL12 mRNA (15 µg mRNA/mouse). On day 4, mice were administered 100 µL of anti-PD-L1 antibody (100 µg/mouse, dissolved in PBS) via subcutaneous injection. Control groups included an anti-PD-L1-only group (n=3) and an untreated group (n=3). Tumor growth was monitored using digital calipers, and tumor volume was calculated using the formula:$V = 0.5 * L * W^2$, where L and W represent the tumor's length and width respectively. Tumor measurements were recorded every 2–3 days from day 3 to day 14. On day 14, mice were euthanized, and tumors were excised for analysis.

For biosafety evaluation, mice (n=3) received a 100 µL subcutaneous injection of PFHA-PEI-mRNA-HP loaded with EGFP mRNA (15 µg mRNA/mouse). Untreated mice (n=3) were used as control. Mice body weight was measured at day 0, day 1 and day 14. Blood samples were collected via submandibular puncture and subjected to blood chemistry analysis (Moichor, San Francisco, CA, USA) to evaluate key biochemical markers, including glucose (GLU), blood urea nitrogen (BUN), albumin (ALB), alanine aminotransferase (ALT), and aspartate aminotransferase (AST).

2.17 Statistical Analysis

The results are presented as mean values ± standard error of the mean. The statistical differences were determined by two-sided unpaired Student's t-test in most of the analysis, except the figure 9d where one way ANOVA with Tukey's HSD Post Hoc Test was applied. The values were considered statistically significant at $p < 0.05$. In figure presentation, n.s. means statistically not significant, * means $p < 0.05$, ** means $p < 0.01$, *** means $p < 0.001$.

3. Results and Discussion

3.1 Design and Synthesis of PFHA-PEI-mRNA-HP

The molecular properties such as molecular weight, polarity and functional groups of each of PFHA-PEI-mRNA-HP's constituent were taken into consideration for selection. PFHA was chosen based on the consideration of appropriate PFHA chain length as PFHA being too long would compromise mRNA complex's aqueous solubility while too short would diminish PFHA's utility in the system. Branched PEI with 2 kDa molecular weight was selected for its relatively strong nucleic acid condensing capability and innocuous toxicity profiles. Given that high molecular weight heparin could compete with mRNA for electrostatic binding and cause large-size aggregation, HP was chosen due to its small size which is beneficial for controlling the size and integrity of mRNA complex. PFHA was conjugated on PEI (branched, MW 2kD) via EDC/NHS coupling chemistry (**Figure 1a**). The PFHA:PEI molar ratio for coupling was set at 7:1 for conjugation as this ratio (i.e., PFHA:PEI/7:1) yielded the best transfection results compared to other ratios (**Figure S1**).

A rotor-syringe mixing (RSM) platform was set up by combining a microliter syringe-loaded syringe pump, a mechanical rotor equipped with a disposable stirring head and a lifting sample tube holder into a solution mixing system to assemble PFHA-PEI, mRNA and HP into PFHA-PEI-mRNA-HP nanoparticles. With precise control over the stirring speed and injection flow rate, the RSM platform ensures consistent mixing efficiency and complexing outcomes when making mRNA complex. The core of nanoparticle is composed of mRNA condensed by PFHA-PEI to render structural compactness for mRNA protection. PFHA-PEI-mRNA complex was first formed by slowly injecting mRNA solution at 1 μL/s into PFHA-PEI solution which was being stirred at 500 RPM by the RSM platform (**Figure 1b**). Injecting mRNA into PFHA-PEI solution instead of the other way around ensures that each individual mRNA molecule can be fully covered and condensed upon contact with PFHA-PEI. The PFHA-PEI:mRNA wt/wt ratio was set at 15:1 for optimal physicochemical properties and transfection compared to other ratios based on the screening results (**Figure S2**).

The surface of the PFHA-PEI-mRNA core is then decorated with HP to form an outer shell layer for tuning the binding tightness of mRNA in the core and in turn facilitating the intracellular delivery of mRNA payload. Pre-calculated amount of HP was then injected into the PFHA-PEI-mRNA solution at 0.5 μL/s while PFHA-PEI-mRNA solution was being stirred at 500 RPM via the same RSM device to complete the formation of PFHA-PEI-mRNA-HP nanoparticles. Since injecting PFHA-PEI-mRNA directly into the HP solution would cause excessive binding of HP onto each individual PFHA-PEI-mRNA complex and result in overwhelming electrostatic binding competition between HP and mRNA, HP was injected into PFHA-PEI-mRNA solution at a slow speed to achieve the gradual HP surface embellishing on PFHA-PEI-mRNA (**Figure 1c**).

3.2 Physicochemical Property Characterization

FTIR and XPS were performed on the purified PFHA-PEI product to confirm the presence of PFHA on PEI after conjugation. The purity of PFHA-PEI was evaluated by high performance liquid chromatography (HPLC). The retention time of PFHA, PFHA-PEI and PEI was 18, 23 and 36 minutes respectively (**Figure S3**). The fact that the PFHA-PEI spectrum did not contain noticeable peaks from pure PFHA and pure PEI suggests the high purity of PFHA-PEI. FTIR analysis revealed the

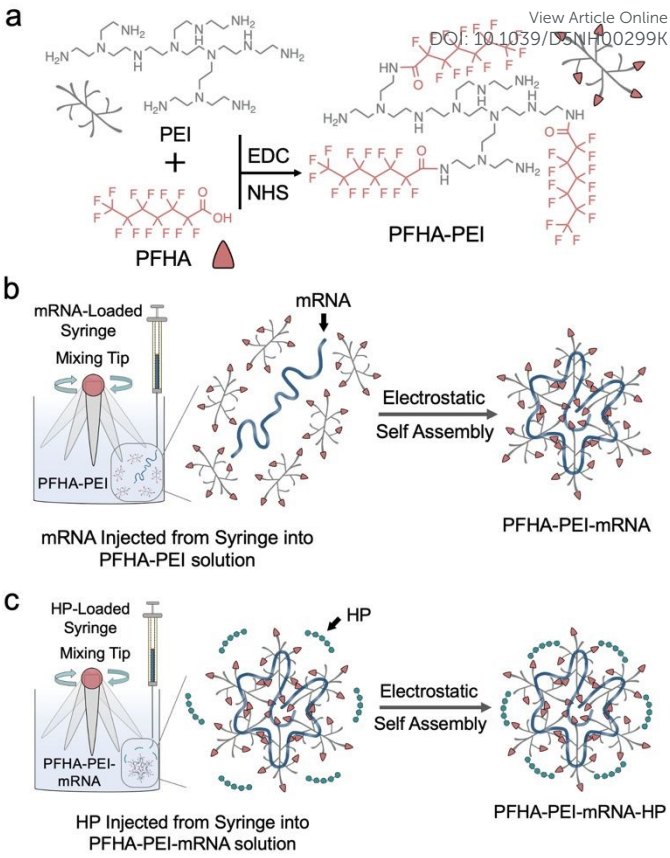

Figure 1. Schematics of the synthesis of PFHA-PEI-mRNA-HP. (a) Reaction scheme for conjugating PFHA onto PEI via EDC/NHS coupling chemistry. For clarity, a monomeric PEI unit is shown rather than the full branched structure of 2 kDa PEI used in synthesis. The schematic depicts conjugation to a primary amine, which is favored due to higher nucleophilicity and accessibility. The PFHA:PEI ratio is not drawn to scale; actual substitution was determined by ^{19}F NMR to be approximately 4.79:1 (see Figure S5). (b) Illustration of the process of mRNA being condensed by PFHA-PEI. mRNA solution was loaded into a syringe and injected into PFHA-PEI solution at a fixed flow rate (1 μL/s) while the solution is stirred by a rotor tip (500 rpm) for homogeneous mixing. (c) Illustration of the process of embellishing the surface of PFHA-PEI-mRNA with HP. HP solution was loaded into a syringe and injected into PFHA-PEI-mRNA solution at a slow flow rate (0.5 μL/s) while the solution is stirred by a rotor tip (500 rpm) for homogeneous mixing.

amide bond formation between PFHA and PEI which was absent from the spectra of pure PFHA or PEI (**Figure 2a**). The unique peak pattern of PFHA was also found adding to PEI's peak pattern in PFHA-PEI's spectrum, indicating successful conjugation of PFHA on PEI. XPS analysis (**Figure 2b**) and Raman spectroscopy analysis (**Figure S4**) of PFHA-PEI also confirmed the presence of the amide bond between PFHA and PEI. The fluorination degree of PEI was characterized by quantitative ^{19}F NMR. With trifluoroacetic acid (TFA) with its characteristic -CF3 peak at –76.15 ppm serving as the internal standard, the unique -CF3 triplet peaks of PFHA on PFHA-PEI at around -82.4 ppm was used to calculate the fluorination degree of PEI.[44] Quantitative results by comparing the integrated area under peaks of -CF3 from PFHA to that from TFA revealed that the PFHA:PEI molar ratio of PFHA-PEI is 4.79:1 (**Figure S5**). These results

collaboratively validated that the synthesis of PFHA-PEI was successful.

Size, surface charge and shape all play critical roles in determining nanoparticle's cellular uptake amount, intracellular fate, and the eventual success of payload delivery. Spherical, cationic nanoparticles with 30-150 nm diameter have been shown to have balanced performance in blood/serum stability, cellular uptake amount and endosomal escape efficiency.[45] Hence, hydrodynamic size and surface charge of PFHA-PEI-mRNA-HP nanoparticles were measured to study their suitability for intracellular mRNA delivery. The influence of each component of PFHA-PEI-mRNA-HP nanoparticle on its overall hydrodynamic size and surface charge was investigated. Without PFHA and HP, branched PEI with 2 kDa molecular weight alone couldn't effectively condense mRNA into a compact nanoparticle as PEI-mRNA is larger than 350 nm in diameter with high polydispersity index of >0.4 (**Figure 2c, d**). When PFHA is integrated into the system, PFHA-PEI was able to condense mRNA into a nanoparticle smaller than 100 nm in size with PDI < 0.2. The further incorporation of HP (mRNA:HP wt/wt ratio of 1:1) did not increase the size and PDI of PFHA-PEI-mRNA nanoparticles, indicating that adding HP at this amount did not affect the compactness nor the uniformity of PFHA-PEI-mRNA nanoparticles. The zeta potential measurements yielded a value close to 40 mV for PFHA-PEI-mRNA and PFHA-PEI-mRNA-HP nanoparticles, and a value close to 50 mV for PEI-mRNA is close to 50 mV (**Figure 2e**). It is reasonable that PEI-mRNA would possess slightly higher surface charge due to its much larger size than the other two nanoparticle formulations and hence would carry more positive charges. Although PFHA-PEI-mRNA is much smaller than PEI-mRNA, its zeta potential (between 35 and 40 mV) is only slightly lower than PEI-mRNA's. This phenomenon suggests that PFHA-PEI-mRNA possesses higher charge density than PEI-mRNA. Since structural compactness is challenging to maintain at high charge density due to the repulsion between same charges, additional favorable energy is required to overcome the structurally destabilizing electrostatic repulsion. The addition of a single component, PFHA, helps maintain the compactness of PEI-mRNA complex, indicating that PFHA's tendency to self-assemble could be the driving energy to overcome same charge repulsion in this system. The relatively high surface charge of PFHA-PEI-mRNA may limit its suitability for systemic (e.g., intravenous) administration due to potential rapid clearance by the mononuclear phagocyte system and increased serum protein adsorption. Future studies may explore surface modification strategies, such as PEGylation or charge-shielding polymers, to improve systemic circulation properties if intravenous delivery is pursued.

Since heparin is a polyanion which could compete with mRNA for electrostatic binding and induce the formation of large aggregates between cationic complex due to charge neutralization, it is crucial to tune the amount of HP in mRNA complexes. When added at the desired amount without affecting the overall stability of mRNA complexes, HP could partially shield positive charges on cationic mRNA complexes to increase biocompatibility and alleviate the binding tension between mRNA and cationic polymers to facilitate the release of mRNA for translation in cytoplasm. Nevertheless, over-adding HP can result in mRNA complex destabilization and possibly premature mRNA release. Therefore, different amounts of HP were added to PFHA-PEI-mRNA to create different versions of mRNA complexes to study the upper limit of HP at which PFHA-PEI-mRNA-HP complex would disintegrate. At or below 1:1 wt/wt of mRNA:HP, the results suggest that PFHA-PEI-mRNA-HP retained similar compact size and zeta potential to that of PFHA-PEI-mRNA (**Figure 2c, d and S6**). The size started to increase slightly at 1:1.5 wt/wt of mRNA:HP, indicating slight destabilization in the compactness of PFHA-PEI-mRNA. At 1:2 wt/wt of mRNA:HP, PFHA-PEI-mRNA-HP's size drastically increased from sub-hundred nm to >240 nm and PDI of near 1, indicating highly polydisperse and aggregated NPs (Figure 2c, d). Even though the zeta potential of PFHA-PEI-mRNA-HP at 1:2 wt/wt of mRNA:HP remained at 40 mV, the much larger hydrodynamic size indicates that the charge density was significantly lower than that of nanoparticle at 1:1 wt/wt of mRNA:HP. This data could mean that HP started to destabilize PFHA-PEI-mRNA at mRNA 1:2 HP wt/wt and caused the formation of large aggregates. But mRNA remained largely unexposed as the zeta potential remained in highly positive realm. As the HP amount was further raised to mRNA 1:5 HP wt/wt, PFHA-PEI-mRNA-HP's zeta potential was completely reverted to the negative realm, suggesting the release of large anionic mRNA molecules and full disintegration of PFHA-PEI-mRNA-HP. The hydrodynamic and zeta potential results were corroborated by gel retardation assay. From the gel image (**Figure 2f**), there were noticeable mRNA signals from the wells of PFHA-PEI-mRNA-HP at 1:5 wt/wt of mRNA:HP, which can be attributed to the partial exposure of the released mRNA from this sample. Meanwhile, there was no detectable signal in the wells loaded with PFHA-PEI-mRNA at other mRNA:HP ratios, suggesting that mRNA is well protected and unexposed in these samples. Transfection test with various HP amounts demonstrated that the optimal transfection results were obtained with 1:1 wt/wt of mRNA:HP wt/wt ratio on 2 different cell lines (**Figure S7**). Based on these results, PFHA-PEI-mRNA with 1:1 wt/wt of mRNA:HP can fully condense mRNA and is optimal in terms of size, zeta potential and transfection efficiency.

mRNA encapsulation study was conducted with free mRNA as positive control and PFHA-PEI-HP (HP amount equivalent to that of mRNA:HP wt/wt ratio of 1:1) as mRNA free negative control. PFHA-PEI-mRNA-HP with mRNA:HP wt/wt ratio of 1:1 was selected as testing groups. The encapsulation results suggest that PFHA-PEI-mRNA-HP with mRNA:HP wt/wt ratio of 1:1 was able to achieve mRNA encapsulation efficiency of 89%, which is comparable to other concurrent highly efficient mRNA delivery vehicles (**Figure S8**).[46, 47] Moreover, PFHA-PEI-mRNA-HP with mRNA:HP wt/wt ratio of 1:1 exhibited a serum stability superior to PEI-mRNA and PFHA-PEI-mRNA (**Figure 2g**). PFHA-PEI-mRNA-HP was able to consistently retain its small size in serum-supplemented solution for over 21 days while PFHA-PEI-mRNA and PEI-mRNA showed unstable size fluctuation starting after day 13. This could be attributed to HP's contribution in shielding PFHA-PEI-mRNA-HP from excessive serum protein adsorption to prevent large aggregates. The fact that PEI-mRNA showed a much larger size fluctuation than PFHA-PEI-mRNA suggests that PFHA also contributed to the serum stability of mRNA complex in this case.

TEM imaging was performed to provide visual confirmation of the compact sizes of PFHA-PEI-mRNA and PFHA-PEI-mRNA-HP. PFHA-PEI-mRNA exhibited a relatively uniform size and spherical shape profile, as evidenced from both high and low magnifications in the TEM images (**Figure 2h**). Upon the addition of 1 μg/mL HP, PFHA-PEI-mRNA-HP exhibited similar size and shape profiles to PFHA-PEI-mRNA. Particle size analysis on the low magnification TEM images

revealed that the average dry diameters of PFHA-PEI-mRNA and PFHA-PEI-mRNA-HP were 31.18 nm and 40.52 nm respectively (**Figure 2i**). These observations suggest that the incorporation of HP at this concentration did not destabilize PFHA-PEI-mRNA, indicating the preservation of its original properties. Hydrodynamic size measurement data further supported the finding. However, it was noted that destabilization of these nanoparticles could occur at higher HP concentrations, potentially attributable to the binding competition between the anionic HP and mRNA. The TEM imaging results were able to corroborate with these observations. Starting with just PEI-mRNA complex, the resultant structure was hundreds of nm in size with amorphous shapes (**Figure S9**). The introduction of PFHA led to the formation of a compact spherical nanostructure. This notable transformation in structure could be attributed to PFHA's spontaneous self-assembly as described before. Drastic structural changes of PFHA-PEI-mRNA-HP were observed when the mRNA:HP wt/wt ratio was further increased to 1:2 and eventually 1:5. At 1:2 wt/wt of mRNA:HP, aggregates with sizes far larger than 200 nm and irregular shape were observed (Figure S9). At 1:5 wt/wt of mRNA:HP, clear disintegration of PFHA-PEI-mRNA-HP was observed. These imaging results agree with previous hydrodynamic size and zeta potential results as they all reveal the critical instability point of PFHA-PEI-mRNA-HP at 1:2 wt/wt of mRNA:HP and full disintegration at 1:5 wt/wt of mRNA:HP. Combined with the high mRNA loading efficiency and serum stability, PFHA-PEI-mRNA-HP with mRNA:HP wt/wt ratio of 1:1 was selected as the optimal formulation for downstream studies.

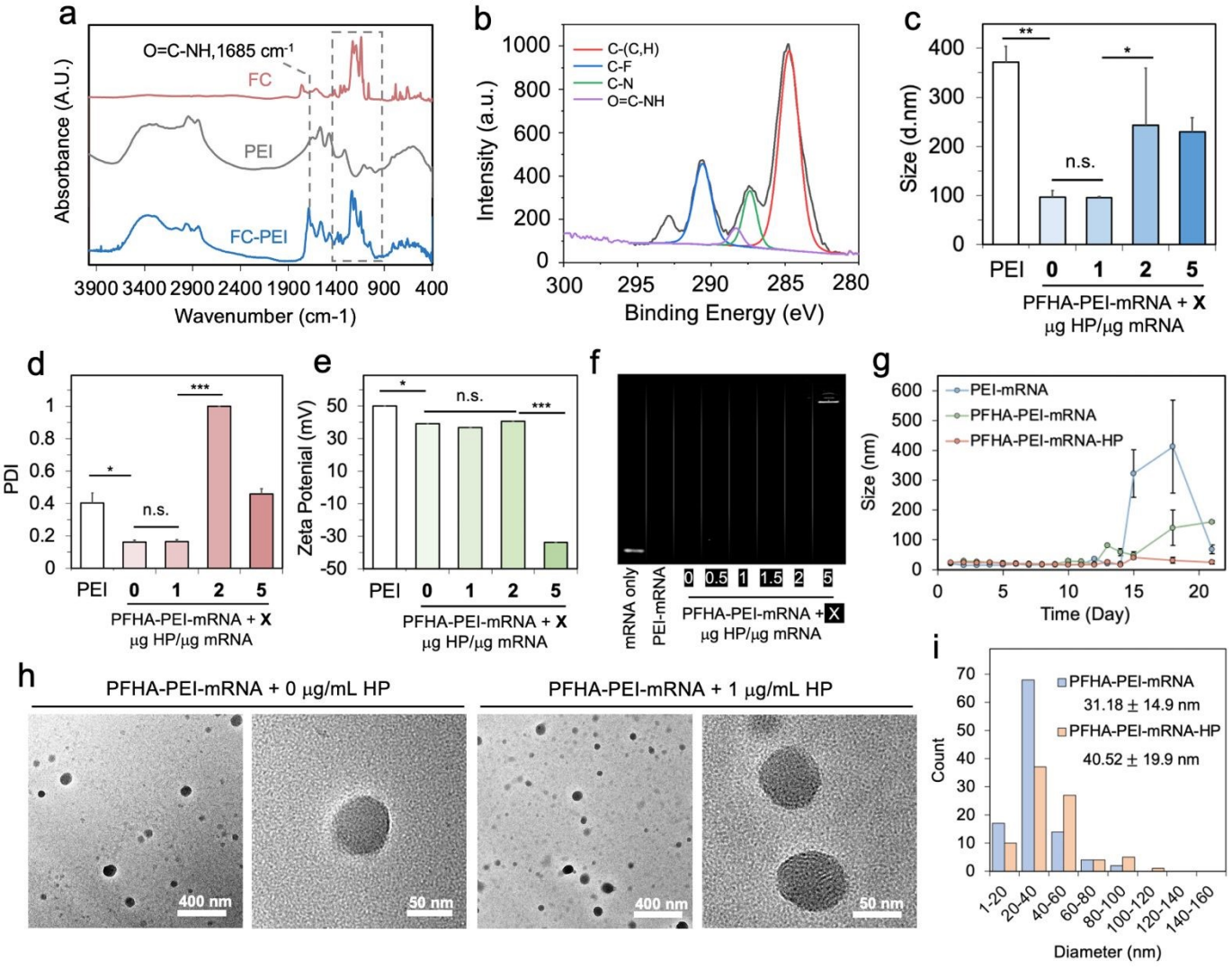

Figure 2. Physicochemical characterization of PFHA-PEI-mRNA-HP. (a) FTIR spectra of PFHA, PEI and PFHA-PEI. The gray dashed box marks the region of the addition of characteristic peak patterns from PFHA's spectrum onto PEI's spectrum. The gray dashed line indicates the presence of the amide bonds formed between PFHA and PEI. (b) X ray photoelectron spectroscopy (XPS) spectrum of PFHA-PEI with peak fitting analysis. Hydrodynamic size (c), polydispersity index (d) and zeta potential (e) measurements of PEI-mRNA, PFHA-PEI-mRNA and PFHA-PEI-mRNA-HP with various HP amounts. For the labels on the x axis of (c) (d) (e), PEI represents PEI-mRNA. 0, 1, 2, 5 correspond to PFHA-PEI-mRNA + 0, 1, 2, 5 μg HP/μg mRNA. (f) Gel retardation assay of PEI-mRNA, PFHA-PEI-mRNA and PFHA-PEI-mRNA-HP (with different HP amounts) with free mRNA as control. (g) Serum stability data of PEI-mRNA, PFHA-PEI-mRNA and PFHA-PEI-mRNA-HP with mRNA:HP wt/wt ratio of 1:1. All samples were placed in PBS supplemented with 10% v/v FBS solutions and incubated at 37 °C. (h) TEM images of PFHA-PEI-mRNA-HP (with different HP amounts) with high and low magnifications. The scale bars are 400 nm and 50 nm respectively. (i) Size distribution profiles of PFHA-PEI-mRNA (no HP) and PFHA-PEI-mRNA-HP NPs from the low magnification TEM images in (h).

3.3 Cellular Uptake and Endosomal Escape

As an essential step toward the downstream transfection success, the cell uptake and endosomal escape performance of PFHA-PEI-mRNA-HP nanoparticle must be evaluated. As a fragile biomolecule prone to degrade, mRNA needs to be protected from RNases during transportation to cell surface, effectively ferried across cell plasma membrane, escape from endo-lysosome to avoid digestion, and eventually released into cytoplasm for translation. Although PFHA-PEI-mRNA-HP shows promising physicochemical properties, its cellular interactions are still largely unknown because nanoparticle's interaction with cells in biological medium is far too complex for mere size, shape, and surface charge profiles to dictate. The avoidance of trapping in digestive lysosomal compartments can be a hallmark of highly efficient transfection agent such as Lipofectamine.[48] Therefore, understanding the cell uptake and the endosomal escape performance is essential for developing successful transfection agents.

4T1 and M6 mouse breast cancer cells are chosen due to their capability to form syngeneic mouse tumors that closely mimic human metastatic breast tumors.[49, 50] In addition, HepG2 human liver cancer cell line is also chosen as it is extensively studied for oncogenesis and drug screening purposes.[51] PFHA-PEI-mRNA-HP with mRNA tagged with Cy5 fluorophores were incubated with 4T1, M6 and HepG2 cancer cells at 37 °C for 12 hours. Lysotracker was added to cell culture 1 hour before the incubation period ends. Z-stacked fluorescent images were utilized and subsequently 3D-rendered into a surface-and-spots model to illustrate precise locations of cell nuclei, mRNA and endo-lysosomes (**Figure 3a**). In these imaging results, the Cy5 signal emitted from PFHA-PEI-mRNA-HP exhibited distinct spatial separation from the lysotracker signal across all three cell lines. This observation suggests that the majority of PFHA-PEI-mRNA-HP did not become trapped in the digestive lysosome.

Cross-sectional views of the 3D images, taken from sagittal, coronal and transverse planes, confirmed the separation between PFHA-PEI-mRNA-HP and lysotracker signals **(Figure 3b)**. A top-down view of the 3D-rendered model was also generated to better reveal the separation between the mRNA Cy5 signal and the lysotracker signal, offering unobstructed perspective (**Figure 3c**). The 3D colocalization analysis revealed that the volumetric Pearson Coefficient between the mRNA and the lysotracker signals was consistently below 0.2 across all three cell lines tested, suggesting that the majority of the mRNA delivered by PFHA-PEI-mRNA-HP successfully escaped from lysosome entrapment, regardless of cell types (Figure 3c).[52, 53]

To investigate the contribution of each component of PFHA-PEI-mRNA-HP to cellular uptake and endosomal escape, PEI-mRNA and PFHA-PEI-mRNA were also loaded with Cy5-tagged mRNA and incubated with all three cell lines for comparative analysis. The images revealed that cells treated with PEI-mRNA exhibited insufficient or negligible cellular uptake, potentially due to the large size of PEI-mRNA and its limited ability to penetrate the plasma membrane (**Figure S10**). Nonetheless, for the minority of PEI-mRNA particles that managed enter the cytoplasm, they demonstrated effective avoidance of colocalization with endolysosomes, likely due to PEI's intrinsic capability to overcome endosomal entrapment.[54]

On the other hand, PFHA-PEI-mRNA demonstrated markedly higher cellular uptake across all 3 cell lines compared to PEI-mRNA. This enhanced uptake can be attributed to PFHA's inherent tendency for self-assembly and its biphasic separation property in both aqueous and organic phase. The compact nature of PFHA-PEI-mRNA allows it to easily traverse lipid-water interface, resulting in a substantial increase in cellular uptake. The unique combination of PFHA's ability for biological membrane penetration and PEI's capability for endosomal escape contributes to the sustained efficiency of PEHA-PEI in evading endosomal entrapment. The introduction of HP further enhances cellular uptake while retaining the rapid endosomal escape characteristic of PFHA-PEI-mRNA. The enhanced intracellular nanoparticle accumulation observed with the addition of heparin is likely due to improved serum stability, as heparin may partially shield the polyplex's positive surface charge and reduce nonspecific adsorption to serum proteins, thereby minimizing premature clearance and allowing more nanoparticles to reach and enter target cells. Another possibility of this higher cell uptake is that HP might slightly loosen PFHA-PEI's binding to mRNA, exposing the mRNA is more prominently for fluorescent detection. In summary, each component of PFHA-PEI-mRNA-HP plays a crucial role in cellular uptake and endosomal escape. PEI contributes endosomal escape capability, PFHA provides efficient biological membrane penetration, and HP enhances cell uptake and mRNA release.

Confocal microscopy images taken at an earlier time point (3 hours post-treatment) for PFHA-PEI-mRNA-HP on 4T1 and HepG2 cells at an mRNA concentration of 2 μg/mL provided further insights into cellular uptake and endosomal escape dynamics (Figure S11). These images show that many nanoparticles are attached to the cell membrane, and partial colocalization with endo-lysosomal compartments can occasionally be observed, particularly in the PFHA-PEI-mRNA-HP group.

A spherical nanoparticle with sub-hundred nm diameter and cationic surface charge typically enters cells via energy-dependent endocytosis. Since PFHA-PEI-mRNA-HP is a cationic spherical nanoparticle with sub-hundred nm diameter and simultaneously possesses hydrophobic moiety PFHA and cell receptor ligand HP, it is expected that PFHA-PEI-mRNA-HP would enter cells via the receptor-mediated energy-dependent endocytosis pathway. As energy-dependent pathways in cells are greatly inhibited at 4°C[55], the internalization of PFHA-PEI-mRNA-HP should be mostly halted at this temperature if endocytosis is responsible for cell uptake in this case. A cellular uptake study where PFHA-PEI-mRNA-HP was applied to all three cell lines and incubate at 4°C was conducted in parallel to the experiments conducted at 37°C to validate this view. Compared to the PFHA-PEI-mRNA-HP nanoparticles that were internalized into deep intracellular space when incubated with cells at 37°C, the imaging results from all 3 cell lines treated at 4°C unanimously show that PFHA-PEI-mRNA-HP nanoparticles were either anchored on the surface of plasma membrane without internalization or only achieved shallow penetration into cytoplasm (**Figure S12**). Notably, the evident lysotracker signal presented in cells incubated at 37 °C mostly disappeared in cells incubated at 4 °C. The fact that the lysotracker signal was barely observable in cells incubated at 4 °C could be the indicator of greatly suppressed endocytosis under this low temperature. These results collectively pointed out that even though PFHA-PEI-mRNA-HP could still bind to cell plasma membrane via electrostatic adsorption at lower temperature, it couldn't be efficiently internalized with endocytosis being effectively halted at 4 °C. Therefore, the energy-dependent endocytosis is primarily responsible for the cellular internalization of PFHA-PEI-mRNA-HP.

3.4 Biocompatibility Tests

PEI-mRNA, PFHA-PEI-mRNA, PFHA-PEI-mRNA-HP and Lipofectamine 2000-mRNA were applied to 4T1, HepG2 and M6 cell lines to assess their biocompatibility based on the quantitative Alamar blue cell viability assay results and observations from bright field cell images. 4T1 cells treated with PFHA-PEI-mRNA-HP were able to retain around 90% viability across the mRNA concentration ranging from 0 to 3 μg/mL (**Figure 4a**). On the other hand, Lipofectamine 2000-mRNA inflicted more than 20% viability loss on 4T1 at 2 μg/mL and above. The toxicity inflicted by PFHA-PEI-mRNA falls between those by PFHA-PEI-mRNA-HP and Lipofectamine 2000-mRNA while PEI-mRNA exerted the highest toxicity on 4T1 by reducing its viability to around 70% at 2 μg/mL and above. On HepG2 cell line, Lipofectamine 2000-mRNA exhibited a clear trend in its toxicity profile. As mRNA concentration increased from 0 to 3 μg/mL, HepG2 cells' viability decreased from 100% to around 70% and eventually 60% (**Figure 4a**).

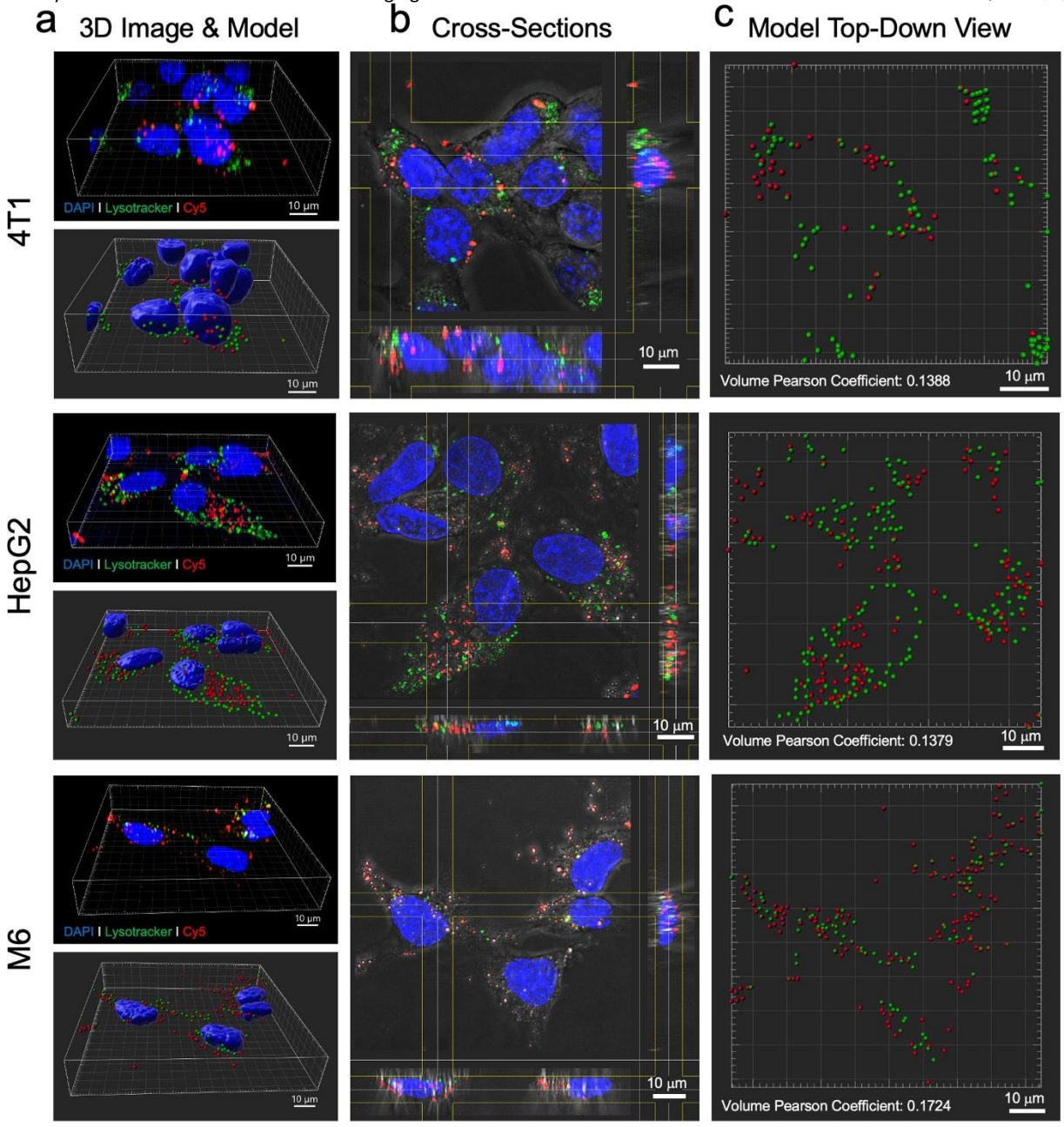

Figure 3. Cell uptake and endosomal escape studies of PFHA-PEI-mRNA-HP on 3 different cancer cell types. All treatments were applied to cells at 37 °C for 12 hours at mRNA concentration of 2 μg/mL 3D Z stacked confocal images were taken with z-resolution of 0.5 μm. The blue color represents cell nuclei; green represents lysotracker and red represents mRNA. (a) Z-stacked 3D images (top panel) and 3D-rendered models (bottom panel) of three cancer cells lines treated with PFHA-PEI-mRNA-HP. In the 3D rendered models, cell nuclei are presented as blue surface, and green and red spots represent endo-lysosomes and mRNA. (b) Cross-sectional images of the z stacked 3D images from (a) viewing from coronal, sagittal and transverse planes with bright field image as background. (c) Top-down view of the 3D-rendered model from (a) excluding cell nuclei. 3D viewing, model rendering and colocalization analysis was performed on the IMARIS image analysis software (Oxford Instruments).

PEI-mRNA treated HepG2 cells consistently showed around 75% viability at mRNA concentration between 0.5 to 3 μg/mL. On the other hand, PFHA-PEI-mRNA or PFHA-PEI-mRNA-HP-treated HepG2 cells were mostly able to retain >80% of viability across 0.5 to 3 μg/mL mRNA concentration. On M6 cell line, cells treated with PFHA-PEI-mRNA exhibited a remarkable retention of viability higher than 90% at 3 μg/mL dose. In comparison, cells treated with PEI-mRNA and PFHA-PEI-mRNA retained ~85% viability. Notably, cells treated with Lipofectamine 2000-mRNA experienced a more significant decline, dropping below 80% viability at the same 3 μg/mL mRNA dose.

The quantitative cell viability assay results were corroborated by bright field images. The bright field images of the untreated or the PFHA-PEI-mRNA-HP-treated 4T1 cells showed similar cell density and morphology, which suggests that the 4T1's proliferation rate and health were not significantly affected by the presence of PFHA-PEI-mRNA-HP (**Figure 4b**). 4T1 cells treated with PEI-mRNA, PFHA-PEI-mRNA and Lipofectamine 2000-mRNA showed slightly lower cell density than the untreated cells, agreeing with 4T1's cell viability results that these treatments had inflicted mild toxicity on 4T1 cells (**Figure 4b and S13**). Although the PFHA-PEI-mRNA-HP-treated HepG2 cells displayed similar cell density as the untreated cell, the morphology of the treated HepG2 appeared to be slightly clumpier and more corrugated than the untreated cells (**Figure 4b**). This corresponds to the slight decrease of viability of the HepG2 cells treated by PFHA-PEI-mRNA-HP at 2 μg/mL mRNA. HepG2 cell images also confirmed that Lipofectamine 2000-mRNA indeed caused noticeable cytotoxicity to HepG2 cells as the cell density was significantly lower and cell morphology appeared to be clumpier. Meanwhile, PEI-mRNA and PFHA-PEI-mRNA only displayed mild adverse effects on HepG2 cells as the cell viability results suggested (**Figure S13**). Bright field images of M6 cells did not show noticeable differences in terms of cell density and morphology between the PFHA-PEI-mRNA-HP-treated, PFHA-PEI-mRNA-treated and the untreated cells, which agrees well with the cell viability test results (**Figure 4b, S13**). One the other hand, M6 cells treated with PEI-mRNA and Lipofectamine 2000-mRNA exhibited lower confluency, along with notable cell shrinkage and clustering. These observations collectively suggest a poorer biocompatibility associated with these two treatments. To validate that the cells visualized in bright field images were indeed viable, Live/Dead staining were performed using Calcein AM and Propidium Iodide (**Figure S14**). The results confirmed that the majority of cells under each treatment condition were alive, further supporting the conclusion that PFHA-PEI-mRNA-HP exhibits minimal cytotoxicity across all tested cell lines.

Taken all the biocompatibility data together, both PFHA-PEI-mRNA-HP and PFHA-PEI-mRNA displayed reliable biocompatibility across all 3 cell lines because they typically inflict less than 20% growth retardation even at mRNA concentration as high as 3 μg/mL. The fact that PFHA-PEI-mRNA-HP-treated cells consistently showed slightly higher viability than that treated by PFHA-PEI-mRNA could suggest HP's contribution in improving mRNA complex's biocompatibility. Without PFHA and HP, PEI-mRNA's toxicity could be obvious on some cell lines. These results indicate that HP and PFHA are both beneficial in alleviating the toxicity from PEI. Although Lipofectamine 2000-mRNA showed decent biocompatibility on 4T1 cells, it inflicted noticeable toxicity on HepG2 and M6 cells at elevated mRNA concentrations so that it can pose safety concerns when applied to certain cell types. Importantly, PFHA-PEI-mRNA-HP also showed promising results in biocompatibility test in mice, suggesting that PFHA-PEI-mRNA-HP could be safe for future in vivo applications.

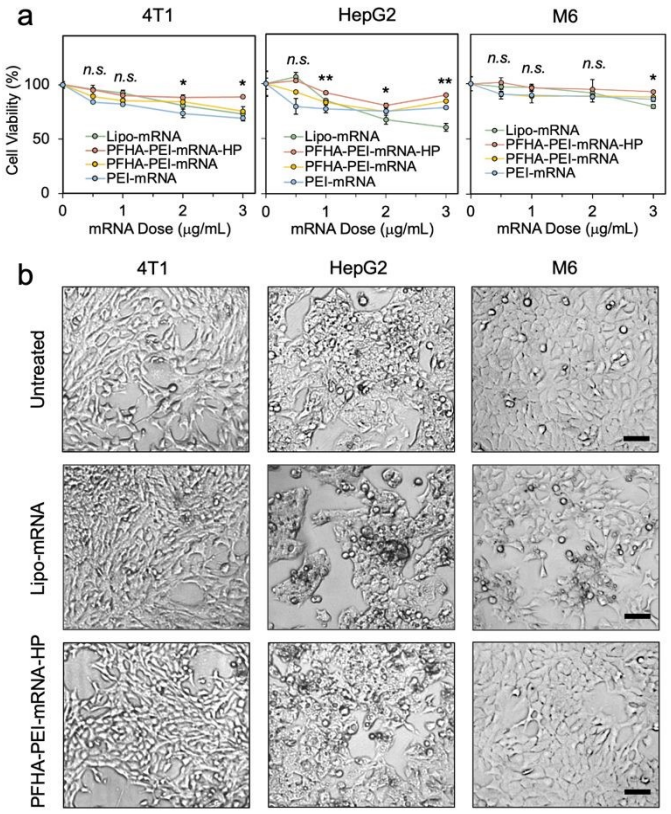

Figure 4. Cell viability test results of PFHA-PEI-mRNA-HP. (a) Quantitative Alamar Blue cell viability assay results on 4T1, HepG2 and M6. Each cell type was treated by PEI-mRNA, PFHA-PEI-mRNA, PFHA-PEI-mRNA-HP and Lipofectamine 2000-mRNA at 0,5, 1, 2 and 3 μg/mL for 24 hours. The untreated cells' viability was normalized to 100% for all cell lines. Statistical analysis was performed to determine if the difference between the data points from the Lipo-mRNA-treated cells and the data points from other treated cells were significant. (b) Representative bright field images of the untreated, Lipofectamine 2000-mRNA-treated and PFHA-PEI-mRNA-HP-treated cells at 2 μg/mL mRNA concentration. Scale bar is 50 μm.

3.5 Transfection Efficiency of Multiple Cell Lines

PEI-mRNA, PFHA-PEI-mRNA, PFHA-PEI-mRNA-HP nanoparticles were applied to 4T1, HepG2 and M6 cell lines to test how each component of PFHA-PEI-mRNA-HP could affect transfection outcomes. The mRNA dosages needed to achieve optimal transfection efficiency on different cell types were determined by dose sensitivity study (**Figure S15**). Through the dose sensitivity study, the mRNA concentration for transfecting all cancer cells was set at 2 μg/mL. As a "gold standard" of commercially available transfection agent touting high transfection efficiency and safety, Lipofectamine 2000-mRNA LNP was used as a positive control for comparison.[48] Based on the fluorescent image results (**Figure 5a, b**), the incorporation of PFHA into PEI-mRNA significantly boosted the mRNA transfection efficiency in all cell lines. The conspicuous improvement in transfection could be attributed to PFHA's inertness, hydrophobicity as well as its lipophobicity. Since it is unfavorable for PFHA to interact with neither polar nor non-polar environment, PFHA can self-assemble into compact structures with itself and remain inert to its ambience. These characteristics render PFHA ideal for protecting fragile payloads such as easily degraded mRNA. The addition of HP to PFHA-PEI-mRNA further significantly enhanced the transfection efficiency on all cell lines. As observed in the previous intracellular trafficking results, the presence of HP significantly increases the cellular uptake of PFHA-PEI-mRNA-HP compared to its counterpart without HP, corroborating HP's enhancement effect on transfection. As observed in the intracellular trafficking results, the addition of HP significantly enhances cellular uptake of PFHA-PEI-mRNA-HP compared to its HP-free counterpart, confirming HP's role in boosting transfection efficiency. This improvement may be attributed to multiple factors, including increased serum stability due to partial shielding of the polyplex's positive surface charge by heparin, which reduce nonspecific adsorption to serum proteins and nanoparticle loss during incubation.

Additionally, previous studies suggest that heparin may bind to fibroblast growth factor receptors (FGFRs), which are often overexpressed in various cancers, potentially facilitating receptor-mediated uptake.[56-58] To investigate this possibility, we performed an FGFR inhibition study using the FGFR inhibitor, PD173074. Cells were pretreated with the inhibitor prior to transfection with PFHA-PEI-mRNA-HP nanoparticles **(Figure S16)**. No significant differences in EGFP expression were observed between FGFR-blocked and unblocked groups in 4T1, HepG2, and M6 cell lines. These results indicate that FGFR is not the primary mediator of cellular uptake in this system. Therefore, the HP-mediated enhancement of delivery is more likely attributed to physicochemical effects such as colloidal stability and charge modulation, rather than specific FGFR interactions.

The mechanism by which heparin enhances transfection may also be attributed to its ability to modulate the electrostatic interactions between the polymer and mRNA, facilitating a subtle packing–unpacking balance that promotes mRNA release in the cytoplasm while still providing sufficient protection during cellular uptake and transport. The exact mechanism, however, remains unclear and requires further investigation as an important direction for future research.

The transfection images show that PFHA-PEI-mRNA-HP was able to achieve comparable transfection efficiency to that of Lipofectamine 2000-mRNA on 4T1, HepG2 and M6 cell lines. These image data combined with the physicochemical profiles of PFHA-PEI-mRNA-HP collectively showcase the importance of well-rounded attributes in size, shape, surface charge, biocompatibility, and intracellular trafficking profiles in successful mRNA transfection. Quantitative flow cytometric analysis was performed to study the percentage of

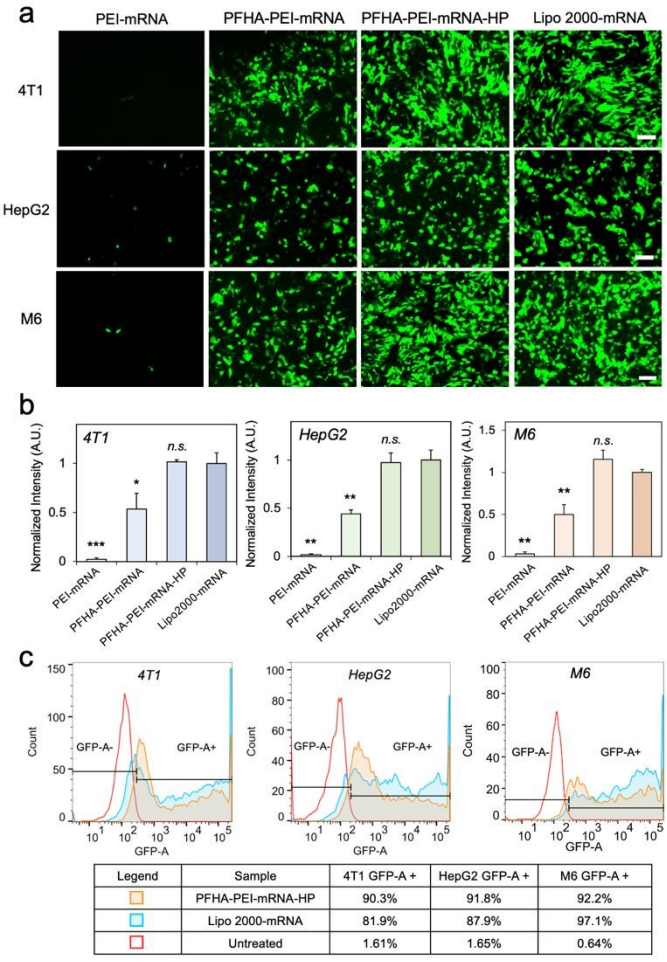

Legend	Sample	4T1 GFP-A +	HepG2 GFP-A +	M6 GFP-A +
	PFHA-PEI-mRNA-HP	90.3%	91.8%	92.2%
	Lipo 2000-mRNA	81.9%	87.9%	97.1%
	Untreated	1.61%	1.65%	0.64%

Figure 5. Transfection results on 3 different cancer cell lines. (a) Transfection images of PEI-mRNA, PFHA-PEI-mRNA and PFHA-PEI-mRNA-HP with Lipofectamine 2000-mRNA as positive control on 4T1, HepG2 and M6 cells. Scale bar is 100 μm. (b) Quantitative analysis of the transfection results presented in (a). Statistical analysis was performed by comparing each of the treatment groups to the positive control lipo2000-mRNA group. (c) Flow cytometric quantitative analysis of transfection efficiency of PFHA-PEI-mRNA-HP with Lipofectamine 2000-mRNA as positive control on 3 cancer cell lines.

successful transfection cell population from each cancer cell line (**Figure 5c**). Similarly, PFHA-PEI-mRNA-HP's transfection performance was compared to Lipofectamine 2000-mRNA in this study. The flow cytometry results showed that PFHA-PEI-mRNA-HP was able to achieve 90.3% and 91.8% transfection efficiency compared to Lipofectamine 2000-mRNA's slightly lower 81.9% and 87.9% on 4T1 and HepG2 cell lines respectively. Meanwhile, PFHA-PEI-mRNA-HP was also able to transfect 92.2% of M6 cell population, slightly lower than Lipofectamine 2000-mRNA's 97.1%.

To further validate the broad applicability of PFHA-PEI-mRNA-HP across different cancer types, three additional cell lines—human breast cancer (MCF7), human brain cancer (SF763), and rat brain cancer (C6)—were subjected to transfection. These cell lines have been extensively utilized in cancer research.[59-61] Consistent with the transfection results observed from 4T1, HepG2 and M6 cells, the addition of PFHA and HP to PEI-mRNA significantly enhanced the transfection efficiency on MCF7, SF763 and C6 cells (**Figure 6a, b**). The flow cytometry analysis showed that PFHA-PEI-mRNA-HP reliably achieved high transfection efficiency of 90.3%, 83.9% and 85.8%, compared to Lipofectamine 2000-mRNA's 71.6%, 87.2% and 79.1%, on MCF7, SF763 and C6 cells respectively (**Figure 6c**). These transfection results collectively demonstrated that PFHA-PEI-mRNA-HP is highly effective in delivering mRNA to various cancer cell types. Moreover, it exhibited similar or even superior performance when compared to the exemplary commercial LNP transfection platform, lipofectamine, across several cell types. These findings position PFHA-PEI-mRNA-HP as a promising polymeric nano-construct candidate for achieving highly efficient mRNA transfection.

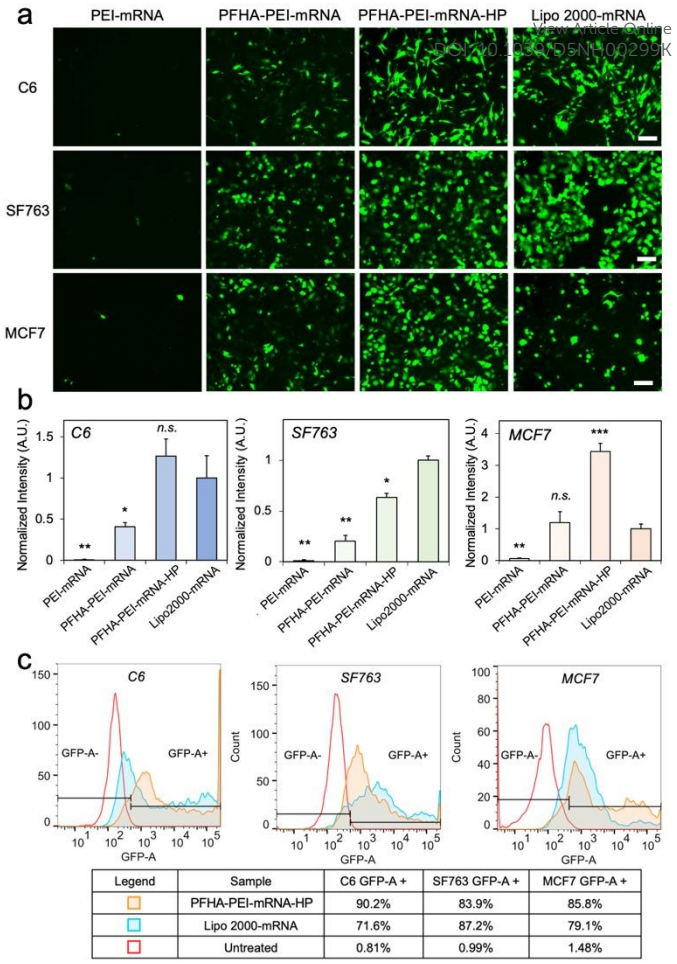

Figure 6. Transfection results on 3 additional cancer cell lines. (a) Transfection images of PEI-mRNA, PFHA-PEI-mRNA and PFHA-PEI-mRNA-HP with Lipofectamine 2000-mRNA as positive control on C6, SF763 and MCF7 cells. Scale bar is 100 μm. (b) Quantitative analysis of the transfection results presented in (a). Statistical analysis was performed by comparing each of the treatment groups to the positive control lipo2000-mRNA group. (c) Flow cytometric quantitative analysis of transfection efficiency of PFHA-PEI-mRNA-HP with Lipofectamine 2000-mRNA as positive control on the additional 3 cancer cell lines.

3.6 Stability of Transfection Efficiency After Storage at 4 °C

The labile nature of mRNA poses significant challenges for storage as it is highly susceptible to nucleases, oxidation, and hydrolysis.[62] Common storage condition for mRNA complexes such as the COVID-19 mRNA vaccines developed by Pfizer-BioNTech and Moderna usually require deep-freezing at –80 °C or –20 °C. These vaccines not only are costly to distribute in cold-chain transportation but also only have narrow window to be administered once thawed, which is usually within hours because frequent freeze-thaw cycle could easily jeopardize the structural integrity of mRNA.[3] Stable storage of mRNA complexes above 0°C without freezing would greatly enhance their usability and transport. Even though lyophilization has been reported to significantly improve mRNA complex's stability at above 0 °C,[63] the additional cost and labor for lyophilization and reconstitution later plus the quality control between these steps may bring more challenges and uncertainties for large-scale processing.

To test whether storing PFHA-PEI-mRNA-HP solution at above 0 °C affects mRNA stability and transfection functionality, PFHA-PEI-mRNA-HP was refrigerated at 4 °C. PFHA-PEI-mRNA-HP samples stored at 4°C were then applied to 4T1 and HepG2 cells for transfection on day 0 (the same day the samples were prepared) as well as on day 1, day 2, day 3, day 4, day 7 and day 15 post sample preparation. Lipofectamine 2000-mRNA was also prepared and stored and tested under similar conditions for comparison. The refrigerated PFHA-PEI-mRNA-HP and Lipofectamine 2000-mRNA sample were allowed to be equilibrated to room temperature before applied to cell culture each time. The results showed that PFHA-PEI-mRNA-HP stored at 4 °C did not show any significant compromise in transfection efficiency on both 4T1 and HepG2 cells for 15 days, indicating that mRNA was well-protected by the PFHA-PEI-HP construct and was able to maintain its structural stability and functionality for prolonged period at 4 °C (**Figure 7a**). On the other hand, the Lipofectamine 2000-mRNA showed significant decrease in transfection efficiency on both cell lines after just one day being stored at 4 °C. Lipofectamine 2000-mRNA lost most of its transfection efficiency after two days of refrigeration, suggesting the Lipofectamine 2000-mRNA is unstable while being stored at 4 °C. Quantitatively, PFHA-PEI-mRNA-HP showed negligible loss of its transfection efficiency on 4T1 cells for 15 days, whereas Lipo-mRNA lost more than 70% of its transfection efficiency on day 1 and furtherly lost 20% more so that the transfection efficiency was only around 5% of that on Day 0 between day 2 and 7 (**Figure 7b**).

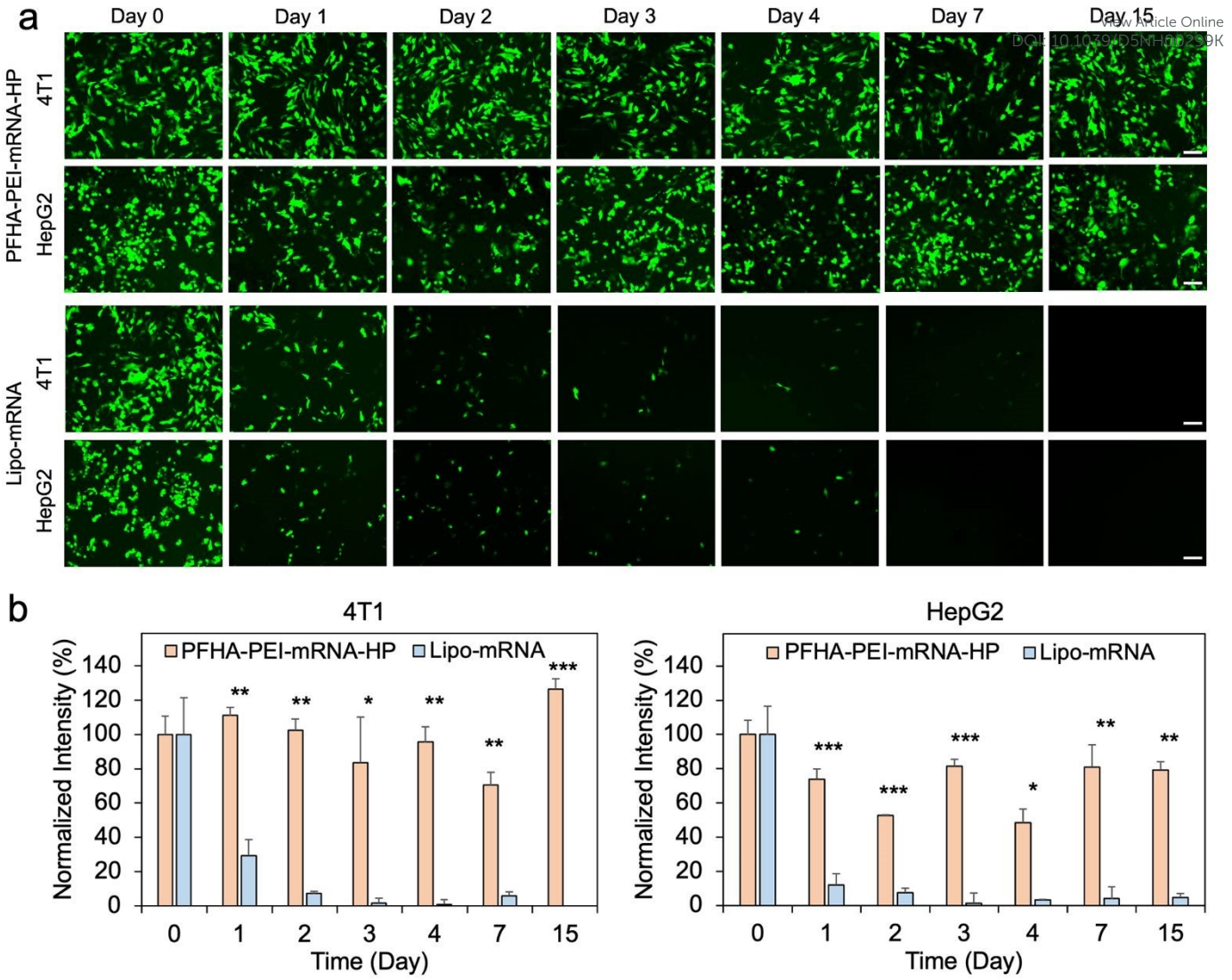

Figure 7. Above 0 °C storage stability test on 4T1 and HepG2 cells. PFHA-PEI-mRNA-HP and Lipofectamine 2000-mRNA were prepared on day 0 and refrigerated at 4 °C throughout the course of study. PFHA-PEI-mRNA-HP and Lipofectamine 2000-mRNA were allowed to equilibrate to room temperature before they were added to 4T1 and HepG2 cell cultures at 2 μg/mL mRNA concentration on day 0, 1, 2, 3, 4, 7 and 15. (a) Fluorescent images of transfected cells. The images were collected 24 hours after PFHA-PEI-mRNA-HP and Lipofectamine 2000-mRNA were added on each day. Scale bar is 100 μm. (b) Quantification of the fluorescence intensities shown in the images. Fluorescence intensities in each panel were normalized against the intensity at day 0 which was assigned as 100%.

In HepG2 cells, PFHA-PEI-mRNA-HP maintained 80% of its transfection efficiency even at day 15 even though the transfection efficiency fluctuated during the study which could be due to variation of HepG2 conditions. On the other hand, Lipo-mRNA lost 90% of its transfection efficiency on HepG2 cells on day 1 and showed no recovery thereafter. Besides hydrolysis, a recent study also showed that the adduct formation between ionizable lipids and mRNA at temperature above 0 °C could compromise the structural integrity of mRNA and cause suppressed protein experssion.[66] Since ionizable lipids are indispensable components in virtually all LNPs, the ionizable lipid-mRNA adduct formation could be one of the factors causing the quick decline in functionality of Lipofectamine 2000-mRNA stored above 0 °C.

3.7. In Vitro Therapeutic mRNA Delivery

For therapeutic mRNA delivery, PFHA-PEI-HP was utilized to deliver IL12-encoding mRNA to 4T1 cells in a proof-of-principle study, with these cells later used in in vivo experiments. Interleukin-12 (IL12), a key cytokine secreted by monocytes and macrophages is one of the pleiotropic cytokines modulating potent activation pathways of essential immune cells such as natural killer (NK) cells, helper and cytotoxic T cells.[64] IL12 also establishes a positive feedback loop with other proinflammatory cytokines including tumor necrosis factor alpha (TNFa) and interferon gamma (IFNg), sustaining the cytotoxic functions of NK cells and T cells.[65]

To evaluate the efficacy of PFHA-PEI-mRNA-HP for delivering therapeutic IL12 mRNA, we encapsulated mouse IL12 mRNA within the nanoparticle system and treated 4T1 cells. As shown in **Figure 8a**, immunofluorescence imaging 24 hours post-treatment

View Article Online
DOI: 10.1039/D5NH00289K

demonstrated strong IL-12 protein expressions (red signal), while no IL-12 signal was detected in untreated controls. The intense red fluorescence observed in treated cells indicates successful intracellular delivery and translation of the mRNA payload. Additionally, ELISA quantification of secreted IL-12 protein in the culture medium confirmed a ~55-fold increase in IL-12 expression in nanoparticle-treated cells compared to untreated controls (**Figure 8b**). These results demonstrate the high efficiency of PFHA-PEI-mRNA-HP in mediating functional mRNA delivery and cytokine production, highlighting its potential utility in cancer immunotherapy applications.

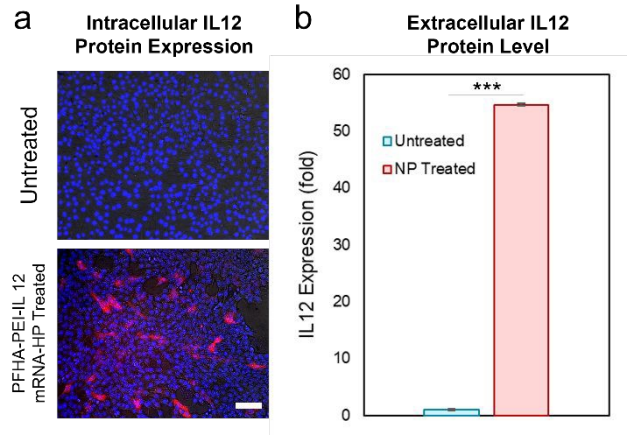

Figure 8. IL12 mRNA delivery to 4T1 cells. (a) Immunofluorescence images showing IL-12 protein intracellular expression on 4T1 cell 24 hours after treatment with PFHA-PEI-IL12 mRNA-HP nanoparticles (bottom) compared to untreated cells (top). Cells were stained with DAPI (blue, nuclei), and IL-12 protein was detected using an anti-IL-12 antibody (red). Scale bar is 100 μm. (b) Quantification of secreted IL-12 protein in culture medium via ELISA. PFHA-PEI-IL12 mRNA-HP nanoparticles treated (NP treated) cells exhibited ~55-fold higher IL-12 expression compared to untreated controls. ***$p < 0.001$.

3.8 In Vivo Therapeutic Efficacy and Biosafety

Given its favorable physicochemical properties, high *in vitro* transfection efficiency, and robust storage stability, the PFHA-PEI-HP mRNA delivery system was evaluated for in vivo therapeutic efficacy to explore its potential for clinical applications. This study utilized the 4T1 triple-negative breast cancer (TNBC) mouse model, which mimics the aggressive nature and treatment challenges of human TNBC, a subtype lacking estrogen, progesterone, and HER2 receptors, making it difficult to target with conventional therapies.[67,68]

Immunotherapy, particularly immune checkpoint inhibitors (ICIs), has shown promise for TNBC by enhancing antitumor immunity through blocking inhibitory T-cell pathways. However, single-agent ICIs, such as anti-PD-L1 therapy, often exhibit limited efficacy in immunosuppressive tumor microenvironments. Combining IL12 with anti-PD-L1 has been shown in preclinical studies to enhance anti- improve immunity and overcome resistance to checkpoint blockade by promoting immune activation.

The 4T1 TNBC model, established by inoculating 4T1 cells into the mammary gland of BALB/c mice, was used due to its similarity to human TNBC, including rapid tumor growth, high metastatic potential, and an immunocompetent microenvironment. To confirm in vivo mRNA delivery, luciferase mRNA (luc mRNA) encapsulated in PFHA-PEI-HP nanoparticles was administered to BALB/c mice (**Figure 9a, 9b**). To minimize mechanical disruption of the tumor and ensure close proximity for diffusion-based delivery, nanoparticles were injected via peritumoral subcutaneous injection rather than intratumorally. This strategy has been adopted in other preclinical models for localized nanoparticle delivery and immunomodulation.[66, 67] Four hours post-injection, luminescence detected via IVIS imaging after luciferin administration confirmed successful mRNA transfection at the tumor site.

Following validation of IL12 mRNA delivery to 4T1 cells in vitro and mRNA (luc mRNA) delivery in vivo, the therapeutic potential of PFHA-PEI-HP was assessed by combining IL12 mRNA delivery with anti-PD-L1 therapy (referred to as "Comb" treatment). The treatment schedule (**Figure 9c**) involved inoculating 4T1 cells on day 0, administering PFHA-PEI-HP with IL12 mRNA subcutaneously on day 3, and injecting anti-PD-L1 on day 4. The dosing regimen was selected based on preliminary internal studies to optimize transfection efficiency, immune activation, and tolerability within a suitable time window. Control groups included anti-PD-L1-only and untreated mice. Tumor volume was monitored from day 3 to day 14 (**Figure 9d**). The Comb group exhibited significant tumor suppression, with 4 of 6 mice tumor-free by day 14 and the remaining two showing minimal tumor growth (**Figure 9e**). In contrast, the anti-PD-L1-only and untreated groups displayed substantial tumor progression.

Although marked tumor suppression was observed following treatment with PFHA-PEI-IL12 mRNA-HP and anti–PD-L1, IL-12 expression in tumor tissues was not directly measured. However, in vitro ELISA results (**Figure 8**) confirmed strong IL-12 protein expression, and in vivo luciferase imaging (**Figure 9b**) demonstrated the platform's ability to deliver and express mRNA in tumors. These findings, alongside observed tumor suppression, suggest that the antitumor effect was likely mediated by IL-12 expression. A further limitation is the lack of an IL-12-only control group, preventing direct comparison of individual versus combined treatment effects. However, prior studies demonstrate enhanced efficacy of IL-12 therapies with PD-L1 blockade, supporting our approach.[68, 69] Additionally, treatment began early (Day 3 post-inoculation) before tumors were fully established or vascularized, enabling evaluation of IL-12 mRNA's immunostimulatory and vaccine-like effects but potentially not reflecting challenges of mature solid tumors. Future studies will incorporate IL-12 monotherapy and delayed treatment in advanced tumor models to clarify each component's role on treatment efficacy in clinically relevant settings.

In addition, biosafety was evaluated through blood chemistry analysis and body weight monitoring. One day after PFHA-PEI-mRNA-HP treatment, the blood chemistry of treated and untreated mice was comparable, with no significant differences observed in albumin (ALB), blood urea nitrogen (BUN), glucose (GLU), alanine aminotransferase (ALT), and aspartate aminotransferase (AST) levels (**Figure 9f**). Additionally, Comb-treated mice maintained stable body weight over two weeks compared to tumor-free mice (**Figure 9g**), indicating no observable systemic toxicity from PFHA-PEI-HP combined with anti-PD-L1.

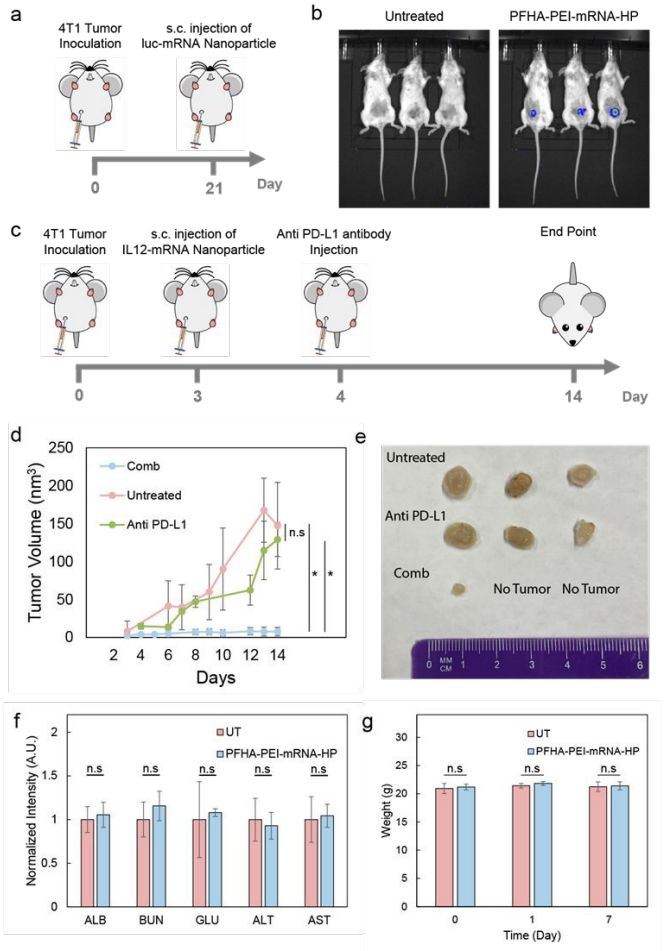

Figure 9. In vivo therapeutic efficacy and biosafety of PFHA-PEI-mRNA-HP nanoparticles. (a) Diagram illustrating the treatment schedule for the in vivo luciferase mRNA transfection study. (b) IVIS imaging of mice 5 hours post-subcutaneous injection of PFHA-PEI-mRNA-HP nanoparticles containing 15 μg luciferase mRNA, with untreated mice as controls. (c) Diagram of the treatment schedule for the in vivo therapeutic study. (d) Tumor volume measurements in mice treated with anti-PD-L1 antibody, IL12 mRNA encapsulated in PFHA-PEI-mRNA-HP nanoparticles, or combination therapy, compared to untreated controls. (e) Representative tumor images from different treatment groups on day 14. (f) Blood chemistry analysis of untreated and PFHA-PEI-mRNA-HP-treated mice. (g) Body weight monitoring of untreated and PFHA-PEI-mRNA-HP-treated mice over the treatment period, showing no significant weight loss.

These results highlight PFHA-PEI-mRNA-HP as a safe and effective platform for mRNA-based immunotherapy, enhancing checkpoint blockade therapy while maintaining a favorable safety profile. This system shows significant promise for clinical translation in TNBC and other aggressive malignancies.

4. Conclusions

This study presented PFHA-PEI-mRNA-HP, a novel polymeric mRNA delivery platform that uniquely combines fluorination and heparinization to overcome limitations of existing gene delivery systems. While fluorination and heparinization have individually enhanced DNA and siRNA delivery, their combined use for mRNA delivery in polymeric carriers is unprecedented. PFHA-PEI-mRNA-HP achieved exceptional transfection efficiency (>90%) across multiple cancer cell lines, surpassing the commercial standard, Lipofectamine 2000. The platform's compact, spherical nanoparticles, enabled by PFHA, addressed PEI's inability to effectively condense mRNA alone. Fluorination enhanced cellular uptake through biphasic separation and bolstered endosomal escape, while heparinization further improved uptake, transfection efficiency, and biocompatibility. These well-balanced physicochemical properties—compactness, cationic surface charge, and robust cellular internalization—underpinned its superior performance.

PFHA-PEI-mRNA-HP demonstrated remarkable versatility, seamlessly accommodating therapeutic mRNA and targeting ligands to enable precise therapeutic applications. In vivo, it efficiently delivered IL12 mRNA, and when combined with anti-PD-L1 therapy, achieved significant tumor suppression in a 4T1 triple-negative breast cancer (TNBC) mouse model. This combination therapy led to complete tumor regression in a subset of treated mice, highlighting its potent antitumor efficacy. Importantly, the platform maintained an excellent safety profile, with no observable toxicity, as evidenced by stable body weight, normal blood chemistry, and absence of adverse effects in treated animals. The synergistic effects of fluorination and heparinization not only enhanced delivery efficiency but also ensured compatibility with biological systems, making PFHA-PEI-mRNA-HP a robust candidate for clinical translation.

Furthermore, PFHA-PEI-mRNA-HP exhibited greater stability than Lipofectamine 2000 when stored above 0°C, suggesting potential for simplified storage and distribution. In conclusion, PFHA-PEI-mRNA-HP represents a highly efficient, stable, and versatile mRNA delivery platform with significant promise for cancer immunotherapy and broader gene therapy applications.

Author Contributions

Conceptualization/validation/methodology/investigation, G.L., J.H., and M.Z.; formal analysis/data curation, G.L., J.H., X.L. and Y.L.; investigation, G.L., J.H., X.L., Y.L., T.J., A.F.and M.Z.; writing—original draft preparation, G.L. and J.H.; writing—review and editing, G.L., J.H. and M.Z.; supervision, M.Z. All authors have read and agreed to the published version of the manuscript.

Conflicts of interest

There are no conflicts of interest to declare.

View Article Online
DOI: 10.1039/D5NH00299K

Acknowledgements

The work was supported by Kuni Foundation and NIH grants (R01EB026890). We acknowledge the use of the equipment on NP characterization from the Nanoengineering and Science Institute and Molecular Engineering and Science Institute supported by NSF (NNCI-2025489, grant NNCI-1542101), UW Department of Chemical Engineering (grant NIH S10 OD030224-01A1), UW W. M. Keck Microscopy Center (grant S10OD016240) and the Department of Pathology's flow cytometry core facility.

References

1. K. A. Hajj and K. A. Whitehead, *Nature Reviews Materials*, 2017, **2**, 1-17.
2. P. S. Kowalski, A. Rudra, L. Miao and D. G. Anderson, *Molecular Therapy*, 2019, **27**, 710-728.
3. X. Hou, T. Zaks, R. Langer and Y. Dong, *Nature Reviews Materials*, 2021, **6**, 1094.
4. R. Tenchov, R. Bird, A. E. Curtze and Q. Zhou, *ACS Nano*, 2021, **15**, 16982-17015.
5. X. Huang, N. Kong, X. Zhang, Y. Cao, R. Langer and W. Tao, *Nature Medicine*, 2022, **28**, 2273-2287.
6. L. Schoenmaker, D. Witzigmann, J. A. Kulkarni, R. Verbeke, G. Kersten, W. Jiskoot and D. J. A. Crommelin, *International Journal of Pharmaceutics*, 2021, **601**, 120586.
7. M. L. Brader, S. J. Williams, J. M. Banks, W. H. Hui, Z. H. Zhou and L. Jin, *Biophysical Journal*, 2021, **120**, 2766-2770.
8. M. Y. Arteta, T. Kjellman, S. Bartesaghi, S. Wallin, X. Wu, A. J. Kvist, A. Dabkowska, N. Székely, A. Radulescu, J. Bergenholtz and L. Lindfors, *Proceedings of the National Academy of Sciences of the United States of America*, 2018, **115**, E3351-E3360.
9. E. Samaridou, J. Heyes and P. Lutwyche, *Advanced Drug Delivery Reviews*, 2020, **154-155**, 37-63.
10. J. Kim, Y. Eygeris, M. Gupta and G. Sahay, *Advanced Drug Delivery Reviews*, 2021, **170**, 83-112.
11. E. Kon, N. Ad-El, I. Hazan-Halevy, L. Stotsky-Oterin and D. Peer, *Nature Reviews Clinical Oncology*, 2023, **20**, 739-754.
12. S. S. Nogueira, A. Schlegel, K. Maxeiner, B. Weber, M. Barz, M. A. Schroer, C. E. Blanchet, D. I. Svergun, S. Ramishetti, D. Peer, P. Langguth, U. Sahin and H. Haas, *ACS Applied Nano Materials*, 2020, **3**, 10634-10645.
13. C. D. Siewert, H. Haas, V. Cornet, S. S. Nogueira, T. Nawroth, L. Uebbing, A. Ziller, J. Al-Gousous, A. Radulescu, M. A. Schroer, C. E. Blanchet, D. I. Svergun, M. P. Radsak, U. Sahin and P. Langguth, *Cells*, 2020, **9**, 2034-2034.
14. S. Iqbal, M. Blenner, A. Alexander-Bryant and J. Larsen, *Biomacromolecules*, 2020, **21**, 1327-1350.
15. C. Zeng, C. Zhang, P. G. Walker and Y. Dong, *Lipid Nanoparticles for Delivery of mRNA Vaccines*, Springer Nature, 2020.
16. M. Zhao, M. Li, Z. Zhang, T. Gong and X. Sun, *Drug Delivery*, 2015, **23**, 2596-2607.
17. M. Li, M. Zhao, Y. Fu, Y. Li, T. Gong, Z. Zhang and X. Sun, *Journal of Controlled Release*, 2016, **228**, 9-19.
18. A. B. Vogel, L. Lambert, E. Kinnear, D. Busse, S. Erbar, K. C. Reuter, L. Wicke, M. Perkovic, T. Beissert, H. Haas, S. T. Reece, U. Sahin and J. S. Tregoning, *Molecular Therapy*, 2018, **26**, 446-455.
19. M. Chiper, N. Tounsi, R. Kole, A. Kichler and G. Zuber, *Journal of Controlled Release*, 2017, **246**, 60-70.
20. E. Lee, A. S. Kamlet, D. C. Powers, C. N. Neumann, G. B. Boursalian, T. Furuya, D. C. Choi, J. M. Hooker and T. Ritter, *Science*, 2011, **334**, 639-642.
21. Y. Takaoka, T. Sakamoto, S. Tsukiji, M. Narazaki, T. Matsuda, H. Tochio, M. Shirakawa and I. Hamachi, *Nature Chemistry*, 2009, **1**, 557-561.
22. Y. Wang, W. C. Lee, K. K. Manga, P. K. Ang, J. Lu, Y. P. Liu, C. T. Lim and K. P. Loh, *Advanced Materials*, 2012, **24**, 4285-4290.
23. W. Liu, X. Huang, M. J. Cheng, R. J. Nielsen, W. A. Goddard and J. T. Groves, *Science*, 2012, **337**, 1322-1325.
24. M. Wang, H. Liu, L. Li and Y. Cheng, *Nature Communications*, 2014, **5**, 1-8.
25. G. Zuo, A. Xie, X. Pan, T. Su, J. Li and W. Dong, *ACS Applied Nano Materials*, 2018, **1**, 2376-2385.
26. H. Wang, Y. Wang, Y. Wang, J. Hu, T. Li, H. Liu, Q. Zhang and Y. Cheng, *Angewandte Chemie*, 2015, **127**, 11813-11817.
27. Y. P. Xiao, J. Zhang, Y. H. Liu, J. H. Zhang, Q. Y. Yu, Z. Huang and X. Q. Yu, *European Journal of Medicinal Chemistry*, 2019, **162**, 602-611.
28. I. T. Horváth and J. Rábai, *Science*, 1994, **266**, 72-75.
29. M. C. Z. Kasuya, S. Nakano, R. Katayama and K. Hatanaka, *Journal of Fluorine Chemistry*, 2011, **132**, 202-206.
30. M. P. Krafft, *Advanced Drug Delivery Reviews*, 2001, **47**, 209-228.
31. L. H. Wang, D. C. Wu, H. X. Xu and Y. Z. You, *Angewandte Chemie International Edition*, 2016, **55**, 755-759.
32. T. Wu, L. Wang, S. Ding and Y. You, *Macromolecular Bioscience*, 2017, **17**, 1700114.
33. S. D. Xiong, L. Li, J. Jiang, L. P. Tong, S. Wu, Z. S. Xu and P. K. Chu, *Biomaterials*, 2010, **31**, 2673-2685.
34. M. E. Johnson, J. Shon, B. M. Guan, J. P. Patterson, N. J. Oldenhuis, A. C. Eldredge, N. C. Gianneschi and Z. Guan, *Bioconjugate Chemistry*, 2016, **27**, 1784-1788.
35. C. Ge, J. Yang, S. Duan, Y. Liu, F. Meng and L. Yin, *Nano Letters*, 2020, **20**, 1738-1746.
36. Z. Zhang, W. Shen, J. Ling, Y. Yan, J. Hu and Y. Cheng, *Nature Communications*, 2018, **9**, 1-8.
37. M. Ahmed and R. Narain, *Biomaterials*, 2013, **34**, 4368-4376.
38. S. P. Strand, S. Lelu, N. K. Reitan, C. D. L. Davies, P. Artursson and K. M. Vårum, *Biomaterials*, 2010, **31**, 975-987.
39. I. Pilipenko, V. Korzhikov-Vlakh, V. Sharoyko, N. Zhang, M. Schäfer-Korting, E. Rühl, C. Zoschke and T. Tennikova, *Pharmaceutics*, 2018, **10**, 117.
40. W. S. Boyle, K. Senger, J. Tolar and T. M. Reineke, *Biomacromolecules*, 2017, **18**, 56-67.
41. O. Jeon, H. S. Yang, T. J. Lee and B. S. Kim, *Journal of Controlled Release*, 2008, **132**, 236-242.
42. H. Sung, J. Ferlay, R. L. Siegel, M. Laversanne, I. Soerjomataram, A. Jemal and F. Bray, *CA: A Cancer Journal for Clinicians*, 2021, **71**, 209-249.
43. K. M. Hotchkiss and J. H. Sampson, *Journal of Neuro-Oncology*, 2021, **151**, 55-62.
44. D. Camdzic, R. A. Dickman and D. S. Aga, *Journal of Hazardous Materials Letters*, 2021, **2**, 100023.

45. E. Blanco, H. Shen and M. Ferrari, *Nature Biotechnology*, 2015, **33**, 941-951.
46. S. Patel, N. Ashwanikumar, E. Robinson, A. Duross, C. Sun, K. E. Murphy-Benenato, C. Mihai, Ö. Almarsson and G. Sahay, *Nano Letters*, 2017, **17**, 5711-5718.
47. C. Fornaguera, M. Guerra-Rebollo, M. Á. Lázaro, C. Castells-Sala, O. Meca-Cortés, V. Ramos-Pérez, A. Cascante, N. Rubio, J. Blanco and S. Borrós, *Advanced Healthcare Materials*, 2018, **7**, 1800335.
48. F. Cardarelli, L. Digiacomo, C. Marchini, A. Amici, F. Salomone, G. Fiume, A. Rossetta, E. Gratton, D. Pozzi and G. Caracciolo, *Scientific Reports*, 2016, **6**, 1-8.
49. Q. Mu, G. Lin, M. Jeon, H. Wang, F. C. Chang, R. A. Revia, J. Yu and M. Zhang, *Materials Today*, 2021, **50**, 149-169.
50. S. E. Stanton, E. Gad, E. Ramos, L. Corulli, J. Annis, J. Childs, H. Katayama, S. Hanash, J. Marks and M. L. Disis, *npj Breast Cancer*, 2021, **7**, 1-9.
51. V. A. Arzumanian, O. I. Kiseleva and E. V. Poverennaya, *International Journal of Molecular Sciences*, 2021, **22**, 13135.
52. J. D. Torres-Vanegas, J. Cifuentes, P. R. Puentes, V. Quezada, A. J. Garcia-Brand, J. C. Cruz and L. H. Reyes, *Frontiers in Chemistry*, 2022, **10**, 1169.
53. B. Smolková, T. MacCulloch, T. F. Rockwood, M. Liu, S. J. W. Henry, A. Frtús, M. Uzhytchak, M. Lunova, M. Hof, P. Jurkiewicz, A. Dejneka, N. Stephanopoulos and O. Lunov, *ACS Applied Materials and Interfaces*, 2021, **13**, 46375-46390.
54. D. Pei and M. Buyanova, *Bioconjugate Chemistry*, 2019, **30**, 273-283.
55. Z. He, K. Liu, E. Manaloto, A. Casey, G. P. Cribaro, H. J. Byrne, F. Tian, C. Barcia, G. E. Conway, P. J. Cullen and J. F. Curtin, *Scientific Reports*, 2018, **8**, 1-11.
56. Y. Ping, Q. Hu, G. Tang and J. Li, *Biomaterials*, 2013, **34**, 6482-6494.
57. R. Porta, R. Borea, A. Coelho, S. Khan, A. Araújo, P. Reclusa, T. Franchina, N. Van Der Steen, P. Van Dam, J. Ferri, R. Sirera, A. Naing, D. Hong and C. Rolfo, *Critical Reviews in Oncology/Hematology*, 2017, **113**, 256-267.
58. L. Pellegrini, D. F. Burke, F. Von Delft, B. Mulloy and T. L. Blundell, *Nature*, 2000, **407**, 1029-1034.
59. R. F. Barth and B. Kaur, *Journal of Neuro-Oncology*, 2009, **94**, 299-312.
60. A. V. Lee, S. Oesterreich and N. E. Davidson, *JNCI: Journal of the National Cancer Institute*, 2015, **107**, 73.
61. X. Zheng, G. Shen, X. Yang and W. Liu, Cancer Research, 2007, 67, 3691-3697.
62. M. N. Uddin and M. A. Roni, Vaccines, 2021, 9, 1033.
63. H. Muramatsu, K. Lam, C. Bajusz, D. Laczkó, K. Karikó, P. Schreiner, A. Martin, P. Lutwyche, J. Heyes and N. Pardi, Molecular Therapy, 2022, 30, 1941-1951.
64. A. E. Barberio, S. G. Smith, I. S. Pires, S. Iyer, F. Reinhardt, M. B. Melo, H. Suh, R. A. Weinberg, D. J. Irvine and P. T. Hammond, Bioengineering & Translational Medicine, 2023, 8, e10453.
65. J. Hodge-Dufour, M. W. Marino, M. R. Horton, A. Jungbluth, M. D. Burdick, R. M. Strieter, P. W. Noble, C. A. Hunter and E. Puré, Proceedings of the National Academy of Sciences of the United States of America, 1998, 95, 13806-13811.
66. H. Shen, Q. Gao, Q. Ye, S. Yang, Y. Wu, Q. Huang, X. Wang and Z. Sun, Int J Nanomedicine, 2018, 13, 7409-7426.
67. Q. G. Wright, D. Sinha, J. W. Wells, I. H. Frazer, J. L. Gonzalez Cruz and G. R. Leggatt, J Immunother Cancer, 2024, 12.
68. J. Lakshmipathi, S. Santha, M. Li, Y. Qian, S. F. Roy, N. Lubeski, K. Politi, M. Bosenberg, J. Eyles and V. Muthusamy, Cancer Immunol Immunother, 2025, 74, 250.
69. C. Xu, Y. Zhang, P. A. Rolfe, V. M. Hernández, W. Guzman, G. Kradjian, B. Marelli, G. Qin, J. Qi, H. Wang, H. Yu, R. Tighe, K. M. Lo, J. M. English, L. Radvanyi and Y. Lan, Clin Cancer Res, 2017, 23, 5869-5880.

View Article Online
DOI: 10.1039/D5NH00299K

New Concepts

This research presents an innovative polymeric mRNA delivery platform that addresses key limitations of lipid nanoparticles (LNPs), widely used in mRNA therapeutics. Despite their clinical success, LNPs rely on complex multicomponent lipid formulations, labor-intensive screening, and cold-chain storage, resulting in batch inconsistencies and high costs. Limited lipid reactive sites also restrict functionalization for targeted therapies. PFHA-PEI-mRNA-HP, based on a single, fluorinated, and heparinized low molecular weight PEI macromolecule, forms cationic nanoparticles that self-assemble with mRNA via simple mixing, enhancing scalability, affordability, and consistency. Fluorination boosts cellular uptake and endosomal escape, while heparinization improves biocompatibility and stability. The platform outperforms Lipofectamine 2000 in transfection efficiency across cancer cell lines and remains stable without cold storage. In vivo, it effectively delivers IL12 mRNA, suppressing triple-negative breast cancer in mice alongside anti-PD-L1 therapy without toxicity. This study not only provides insights of designing and optimizing a novel polymeric mRNA delivery platform but also conceptually demonstrated the promising utility of functionalized cationic polymers in the field of mRNA delivery.

View Article Online
DOI: 10.1039/D5NH00299K

Data availability statement

We confirm that all the relevant research data is contained with the manuscript and electronic supplementary information (ESI). No databases have been used and no references to such databases are contained in the manuscript or ESI.